

Mutant Screen Reveals the *Piccolo's* Control over Depression and Brain-Gonad Crosstalk

Gerardo A. Medrano^{1&}, Manvendra Singh^{11&}, Erik J. Plautz⁶, Levi B. Good⁶, Karen M. Chapman¹, Jaideep Chaudhary¹, Priscilla Jaichander¹, Heather M. Powell¹, Ashutosh Pudasaini², John M. Shelton³, James A. Richardson^{4,5}, Xian-Jin Xie⁷, Zoltán Ivics⁹, Christine Braun¹⁰, Frauke Ackermann¹⁰, Craig C. Garner¹⁰, Zsuzsanna Izsvák^{11,*} and F. Kent Hamra^{1, 2, 8,*}

Departments of Pharmacology¹, Obstetrics & Gynecology², Internal Medicine - Division of Cardiology³, Pathology⁴, Molecular Biology⁵, Neurology and Neurotherapeutics⁶, Simmons Comprehensive Cancer Center⁷, Cecil H & Ida Green Center for Reproductive Biology Sciences⁸, University of Texas Southwestern Medical Center in Dallas, USA; Paul-Ehrlich-Institute, Division of Medical Biotechnology, Langen, Germany⁹, German Center for Neurodegenerative Diseases (DZNE), Charité Medical University, Charitéplatz 1, 10117 Berlin, Germany¹⁰, Max Delbrück Center for Molecular Medicine in the Helmholtz Society, Berlin, Germany¹¹

equal contribution &

*Address Correspondence to:

F. Kent Hamra
Department Obstetrics and Gynecology
Cecil H & Ida Green Center for
Reproductive Biology Sciences
UT Southwestern Medical Center
5323 Harry Hines Blvd.
Dallas, Texas 75390

Telephone: (214) 645-6279
Fax: (214) 645-6276
Email: kent.hamra@utsouthwestern.edu

Zsuzsanna Izsvák
Max Delbrück Center for Molecular Medicine
in the Helmholtz Society
Robert Rössle Str. 10
D-13092 Berlin, Germany

Telephone: (49) 30 9406-3510
FAX: (49) 30 9406-2547
Email: www.mdc-berlin.de/izsvak

Key Words: reproduction, social behavior, affective disorders, con-specific recognition, mating, aggression, depression, seizures, epilepsy, GABAergic, olfactory, hypothalamus, amygdala, forward genetics, *Sleeping Beauty* transposon, gene-trap, mutagenesis, pleiotropy, spermatogonial, spermatogenesis, acrosome reaction, knockout rats, autophagy

Running Title: Rat Genetics Unveils *Pclo* Pleiotropy

Abstract

Successful sexual reproduction involves a highly complex, genetically encoded interplay between animal physiology and behavior. Here we developed a screen to identify genes essential for rat reproduction based on an unbiased methodology involving mutagenesis via the *Sleeping Beauty* transposon. As expected, our screen identified genes where reproductive failure was connected to gametogenesis (*Btrc*, *Pan3*, *Spaca6*, *Ube2k*) and embryogenesis (*Alk3*, *Exoc6b*, *Slc1a3*, *Tmx4*, *Zmynd8*). In addition, our screen identified *Atg13* (longevity) *Dlg1* and *Pclo* (neuronal disorders), previously not associated with reproduction. Dominant *Pclo* traits caused epileptiform activity and affected genes supporting GABAergic synaptic transmission (*Gabra6*, *Gabrg3*), and animals exhibited a compromised crosstalk between the brain and gonads via disturbed GnRH signaling. Recessive *Pclo* traits disrupted conspecific recognition required for courtship/mating and were mapped to allelic markers for major depressive disorder (*Grm5*, *Htr2a*, *Sorcs3*, *Negr1*, *Drd2*). Thus, *Pclo*-deficiency in rats link neural networks controlling sexual motivation to *Pclo* variants that have been associated with human neurological disorders.

Introduction

While a failure to reproduce sexually is often connected to physiological or developmental problems of the gonad, gamete or embryo, it is also commonly accepted that problems with sexual reproduction can be linked to various behavioral abnormalities^{1, 2}. Indeed, inborn social behaviors related to sex, defense and maternal care are regulated by the central nervous system to ensure reproduction^{3, 4}.

From the hundreds of genes essential for neuroendocrine/gonadal control over gametogenesis and fertilization^{5, 6}, neurotransmission genes that govern sensory neuron-stimulated social behavior mediate the primary signals that initiate reproduction^{3, 4}. Instinctive social responses such as pleasure, attraction, fear, aggression and avoidance that affect reproduction are processed by the limbic system to modulate motivational responses^{3, 4, 7, 8}. Innate reproductive behaviors are driven by afferent sensory neurons that innervate the limbic system in mammals and are driven by sex and sex hormones (estrogen and testosterone)^{3, 4}. Abnormalities in the cortico-limbic networks that integrate survival-driven reproductive behavior with emotional awareness and memory play crucial roles in the etiology of human “affective disorders”^{7, 8}, including depression, bipolar disorder, autism, anxiety and addiction, and represent neurological health conditions.

In this study, we aimed to identify novel genes required for reproduction. Our intention was to reach out from the circle of the obvious candidates and uncover novel layers of complexity (e.g. reproductive behavior), remaining as open as possible to the unexpected. Our

experimental strategy followed from this decision. We chose an unbiased forward mutagenesis strategy instead of a targeted approach.

Rats provide various advantages over mice in modeling both human reproduction and behavior. In rodents, sensory input to the limbic system is mediated predominantly via the olfactory system [olfactory epithelia > olfactory nuclei > main and/or accessory olfactory bulb > medial amygdala > bed nucleus of stria terminalis > medial pre-optic hypothalamic nucleus]^{3, 4}. Pheromones associated with mating bind olfactory receptors in the olfactory epithelium and elicit pre-copulatory social behaviors such as partner investigation, grooming and courtship. These activities culminate in copulatory and post-copulatory behaviors^{3, 4}. Notably, the rat's olfactory epithelium is uniquely endowed with ~1,400 genes encoding olfactory receptors⁹ and has long provided an experimental system to study the mechanisms by which sensory inputs stimulate social behavior that affect reproduction, self-defense and parental care^{3, 4}.

Sleeping Beauty genetraps insertions occur randomly¹⁰. We previously reported on a method based on spermatogonial stem cell libraries harboring *Sleeping Beauty* genetraps insertions that can streamline the large-scale production of knockout rats for genetic assays^{11, 12}. In the current study, a panel of 12 novel, pre-selected *Sleeping Beauty* rat strains derived from a spermatogonial genetraps library¹² were tested for impaired reproductive behavior phenotypes. Our strategy proved to be successful: in addition to the candidate genes and phenotypes, our screen identified unexpected determinants of reproductive success. In addition to genes required for gamete and embryo development, our screen unveiled deep-

seated connections between reproduction, fitness and social behavior. Among the reproduction genes, we identified *Atg13*, which has generally been connected to longevity in species ranging from yeast to plants and humans. We additionally identified *Pclo*-deficient phenotypes, which have previously been reported in humans with inherited forms of affective disorders and central atrophy¹³⁻¹⁷. In doing so, we report robust behavior-based forward genetics in the rat that led us to define *Pclo* as a neuronal determinant essential for integrating sensory information with social acuity.

Results

A set of mutations affects reproduction

To identify reproductive genes, we used a forward genetics approach in mutant rats produced from a donor spermatogonial stem cell library (Fig. 1). Each individual mutant strain derived from the spermatogonial library harbored a *Sleeping Beauty* genetrapped transposon within a distinct protein coding gene (Supplementary Fig. 1 and Supplementary Table 1). *Sleeping Beauty* mutant strains were analyzed for their ability to reproduce after pairing with wildtype (wt) breeders (Fig. 2a and Supplementary Table 2). An inability to reproduce was linked to a variety of phenotypes that included gametogenesis defects (*Btrc*^{gt/gt}, *Ube2k*^{gt/gt}, *Pan3*^{gt/gt}, *Spaca6*^{gt/gt}), embryonic lethality (*Alk3*^{gt/gt}, *Exoc6b*^{gt/gt}, *Slc1a3*^{gt/gt}, *Tmx4*^{gt/gt}, *Zmynd8*^{gt/gt}), end-stage organ failure (*Atg13*^{gt/gt}) and impaired behavior (*Pclo*^{gt/gt} and *Dlg1*^{wt/gt}) (Supplementary Tables 3-4). In total, 12 genes proved to be essential for reproduction (See *Supplementary Material* for complete reproductive phenotyping).

Mutations that disrupt distinct steps in rat spermatogenesis

Homozygous genetrapped mutations in *Btrc*, *Ube2k* and *Pan3* blocked spermatogenesis at pre-meiotic, meiotic and post-meiotic steps, respectively (Figs. 2b and Supplementary Fig. 2a, b). Only residual numbers of malformed spermatozoa were detected in *Btrc*^{gt/gt} males, and no epididymal spermatozoa were observed in *Ube2k*^{gt/gt} or *Pan3*^{gt/gt} males (Supplementary Fig. 3). In corresponding *Ube2k*^{gt/gt}, *Btrc*^{gt/gt} and *Pan3*^{gt/gt} genotypes, spermatogenic arrest was reflected by reduced testis size (Fig. 2c and Supplementary Table 3).

A group of mutant rats develop gametes, but do not reproduce

By contrast, rats with homozygous mutations in the *Spaca6*, *Atg13* and *Pclo* genes produced both eggs and sperm (Supplementary Figs. 2 and 3). However, neither sex of *Atg13*^{gt/gt} and *Pclo*^{gt/gt} rats were able to reproduce, as was the case with *Spaca6*^{gt/gt} males (Fig. 2a and Supplementary Table 2). While *Spaca6*^{gt/gt} epididymides had slightly reduced numbers of spermatozoa (Supplementary Fig. 3), their moderate deviation in sperm counts could not explain the infertility phenotype we observed. Furthermore, *Spaca6*^{gt/gt} male mating behavior was normal compared to wt males, as supported by the presence of spermatozoa in vaginal swabs (n=4 breeder pairs). Accordingly, in mutant mice lacking a 11kb region of chromosome 17, *Spaca6* was initially implicated in gamete membrane fusion¹⁸. As with *Spaca6*^{gt/gt} males, the inability of *Atg13* and *Pclo* homozygous mutants to reproduce could not be explained by an early blockage of gamete production, and therefore required further analyses.

Reproduction defects in *Atg13* mutants correlate with reduced longevity.

Whereas *Autophagy related 13* (*Atg13*) is required for autophagic flux and reaching an optimal lifespan in plants and animals (Supplementary Table 4)¹⁹⁻²², the role of *Atg13* in additional reproduction-related traits is unknown. All male *Atg13*^{gt/gt} mutants were characterized by reduced epididymal sperm counts (Supplementary Fig. 3). *Atg13*^{gt/gt} cauda epididymal spermatozoa flagella were immotile and displayed more detached heads and tails than WT (n=4/genotype). The insertional mutation resulted in a truncated form of ATG13, predicted to lack 25 carboxyl-terminal amino acids encoded by exon 16 (Fig. 3a and Supplementary Table 1). The expression of truncated ATG13 resembled that of WT ATG13: it was abundant in testes, with lower levels in other tissues (Fig. 3a, inset).

Notably, all *Atg13^{gt/gt}* rats inherited pathologies associated with premature death at 3-5 months of age (Fig. 3b). The livers and kidneys of *Atg13^{gt/gt}* rats were abnormal (Fig. 3c). In the liver, cells scattered throughout histological sections contained small spherical vacuoles, consistent with an accumulation of triglycerides (Supplementary Fig. 4a). All the kidneys that were examined displayed marked glomerulonephritis and moderate tubule interstitial disease (Fig. 3d and Supplementary Fig. 4a). Homozygous *Atg13^{gt/gt}* animals (n=3) from one of three pedigrees also demonstrated edematous paws and digits in adult animals (Fig. 3e).

Consistent with the biological functions of *Atg13*, disruptions in the relative abundance of autophagy markers LC3a-I/II and p62 were found in *Atg13^{gt/gt}* embryonic fibroblasts (Fig. 3f and Supplementary Fig. 4b). Thus, the reproduction defects in both female and male *Atg13^{gt/gt}* rats correlated with adult-lethal pathologies, and in males, *Atg13^{gt/gt}* was further associated with abnormal spermatozoa.

Compromised neurotransmission in *Pclo* mutants

Pclo^{gt/gt} animals harbor the *Sleeping Beauty* genetrapp in *Pclo* intron 3, deleting exons 4-25 (*Pclo^{SBA4-25}*) (Fig. 4a). *Pclo* encodes multiple protein isoforms (70-560kDa) that are primarily localized in the cytomatrix of pre-synaptic neurons and have been implicated playing a key role in synaptic transmission²³⁻²⁷. Piccolo is expressed in various tissues and is enriched in the brain (in regions such as the cerebellum, nucleus accumbens, frontal cortex, hypothalamus, and pituitary gland: [GTEX Portal PCLO](#)). Despite their reproductive failure (Fig. 2a), *Pclo^{gt/gt}* mutant animals did not display any obvious dysfunction during gametogenesis (Supplementary Fig. 2). The numbers of epididymal spermatozoa from *Pclo^{gt/gt}* rats were relatively normal (Supplementary Fig. 3a). However, spermatozoa from

Pclo^{gt/gt} rats were not found in vaginal swabs of WT females (6 of 6 breeder pairs) (Fig. 4b), and spermatozoa from WT males were not detected in *Pclo*^{gt/gt} females (6 of 6 breeder pairs) (Fig. 4b). We took these results alongside with the known predominant distribution of *Pclo* transcripts in the brain and hypothesized that the reproductive failure of the *Pclo*^{gt/gt} line might be connected to neurological deficits rather than any physiological abnormality of the gonads.

To gain insights into Piccolo's role in reproductive phenotypes, high-throughput RNA sequencing (RNA-seq) was carried out on testes and brain tissues from *Pclo*^{gt/gt}, *Pclo*^{gt/wt} and *Pclo*^{wt/wt} animals (~6 mo old). *Pclo* transcripts are readily detectable in the brain, whereas the testicular expression of *Pclo* is low (< 0.1 FPKM) (Supplementary Table 5). In the brain, the genetrapp insertion reduced *Pclo* expression to the point that it was undetectable (< 0.1 FPKM) in homozygous *Pclo*^{gt/gt} animals, while no significant transcriptional changes of *Pclo* could be detected in heterozygous animals (Fig. 4c). Similarly, at the protein level, Piccolo was reduced only in the brains of *Pclo*^{gt/gt} rats (>99%), whereas it was not significantly affected in *Pclo*^{wt/gt} compared to *Pclo*^{wt/wt} littermates (Fig. 4d). Thus, expression from a single *Pclo* allele appears to be sufficient to drive normal levels of the gene product, and the phenotype that was observed appears to be connected to the allelic origin of Piccolo.

Our transcriptome analysis of *Pclo*^{gt/gt} and *Pclo*^{wt/wt} animals revealed a higher number of differentially expressed genes (DEGs) in the brain (754) than testis (88), while 16 genes were affected in both tissues (FPKM > 2 and log₂ fold change |1| and E-FDR < 0.01) (Fig. 4e, Supplementary Table 5). These included *Tspo*, *Tagln2*, *Folr1*, *Adh1*, *Hbb* and *Ces1d*, which are involved in steroid hormone production and transport in the blood stream (Fig. 4e,

Supplementary Table 5). Despite a lack of detectable changes in Piccolo RNA/protein abundance in *Pclo*^{wt/gt} rat brains, 325 genes were differentially expressed (log₂FC |1|) in heterozygotes compared to WT or homozygotes (Fig. 4f, Supplementary Table 5), reflecting robust allelic effects. Interestingly, *Pclo*^{gt/gt} and *Pclo*^{wt/gt} showed a similar pattern of transcriptome change compared with *Pclo*^{wt/wt} (Fig. 4c, Supplementary Table 5).

The Gene Ontology (GO) category most highly associated with the dominant phenotype (DEGs in both *Pclo*^{gt/gt} and *Pclo*^{wt/gt} rats vs *Pclo*^{wt/wt}) was *Synaptic Transmission* (Fig. 5a; Supplementary Table 6). The most significantly affected processes in this category included the *gamma-aminobutyric acid (GABA) signaling pathway* (Fig. 5b, Supplementary Table. 6) (GO:0007214, p=0.0000009). Fittingly, the most significantly affected genes were *Gabra6* (*GABA(A) Receptor Subunit Alpha 6*) in the brain and *Gabrg3* (*GABA(A) Receptor Subunit Gamma-3*) in the testis (Fig. 4f; Supplementary Fig. 5). While *Gabra6* is normally expressed in the cerebellum of the brain ([GTEX Portal Gabra6](#)), *Gabrg3* has a higher enrichment in the testis and only a moderate enrichment in the pituitary gland of the brain ([GTEX Portal Gabrg3](#)). In *Pclo* mutant rats, the expression of both *Gabra6* and *Gabrg3* was reduced in both homo- and heterozygous animals (Supplementary Fig. 5), consistent with a dominant phenotype. Curiously, the expression of both *Gabra6* and *Gabrg3* dropped to undetectable levels in *Pclo* mutant rats, suggesting that the KO *Pclo* genotype results in an expression level close-to KO phenotype for these GABA(A) receptor subunits.

Disturbed hormonal secretion in *Pclo* mutants

In addition to *Synaptic Transmission* gene sets, the Gene Ontology analysis of *Pclo*^{wt/wt} rat brains revealed a prominent cluster of *Hormonal Secretion* gene sets that were

downregulated compared to *Pclo^{gt/gt}* animals (Fig. 5b). A further pathway analysis (PANTHER) revealed that the genes affected by the genetrapped *Pclo* fall most frequently into the major signaling pathways of the *Gonadotropin-releasing hormone (GnRH) receptor*, which plays a fundamental role in reproduction by regulating the hypothalamic-pituitary-gonadal axis²⁸, followed by *Wnt*, *Chemokine-cytokine* and *CCKR* signaling (Supplementary Fig. 6a).

Importantly, the data establish a link between GABA signals and GnRH function²⁹, as a perturbation of GABA signals via GABA receptors is known to affect the rate of synthesis and pattern of release of GnRH^{30,31}. Moreover, the GABA signal, which depolarizes GnRH neurons during development, regulates overall GnRH maturation (e.g. migration to the brain). The composition of GABA(A) receptor subunits affects the process of GnRH-1 maturation³², and *Gabra6* is a receptor subunit within embryonic GnRH-1 neurons, which later in life is replaced by *Gabra2* as these neurons develop³². This led us to wonder whether the close-to-KO *Gabra6* phenotype we observed might alter the migration pattern of the GnRH neurons and thus compromise the establishment of proper GnRH signaling. A direct assessment of GnRH expression in the adult brain of *Pclo^{gt/gt}* rats revealed normal numbers of GnRH immuno-positive cells in the pre-optic area of the hypothalamus (Fig. 5c), and that GnRH-positive axons projected normally into the medial eminence (Fig. 5d, Supplementary Fig. 6b). Thus, lack of GnRH neuron development in the pre-optic area is unlikely to be caused by the *Gabra6* KO phenotype of the *Pclo* mutant animals. This suggests that other receptor subunits might compensate for *Gabra6* functions³³ during the process of GnRH neuron maturation.

While the GnRH signal itself lies below the level of reliable detection in our whole-brain RNA-seq data, mapping the differentially expressed genes (DEGs) in the *Pclo*^{gt/gt} mutant samples on the KEGG database revealed that several components of the GnRH signaling pathway are downregulated compared to *Pclo*^{wt/wt} (Supplementary Fig. 6c, d). The GnRH receptor transmits its signals mainly through *Heterotrimeric G-proteins*, a category that is also significantly affected in *Pclo* mutants (Supplementary Fig. 6a). Our analysis revealed that a major fraction of the G-protein coupled receptors (GPCRs) involved in conducting GnRH signaling on gonadotropes are downregulated in the brains of *Pclo* mutants (Supplementary Fig. 7a). Similarly, the cascade involved in mobilizing Ca²⁺ from InsP₃-sensitive intracellular pools, required for the secretion of gonadotropins, is impaired in these animals [(Supplementary Fig. 7b). A downregulation of these processes might affect the end products of the *GnRH signaling pathway* (e.g. luteinizing hormone, LH; follicle-stimulating hormone, FSH) (Supplementary Fig. 6d).

To follow up on this, we used data mining³⁴ and performed a transcriptome-wide analysis of target genes that might be stimulated or repressed by LH and FSH or regulated by testosterone. Our approach revealed that about half of the genes that were dysregulated in *Pclo* KO testes responded to a particular hormonal stimulation in a reverse order ($\rho = -0.31$ and $p\text{-value} < 2.2e-16$) (Fig. 5e, Supplementary Fig 7c). *Gabrg3*, *Ces1d*, *Card9*, *Insl3* and *Hp* appear among the most affected targets of LH, FSH and testosterone in the testes of the *Pclo* mutants (Fig. 5f). Mis-regulated gonadotropin-responsive testis genes highlight a potential for infertility phenotypes to occur downstream of GnRH signaling in *Pclo*-deficient rats.

Among the genes dysregulated in both *Pclo^{gt/gt}* and *Pclo^{gt/wt}* compared to *Pclo^{wt/wt}* rat brains, we also found an upregulation (~6-fold) of neuropeptide Y (*Npy*), which functions through GPCR signaling (Fig. 4f, Supplementary Table 5). *Npy* is also upregulated in the rat limbic system in response to olfactory bulbectomy (OBx)^{35, 36}. Notably, OBx rats, which are used as a model of depressive disorders^{37, 38}, were reported to display reduced sexual motivation, highlighting the complexity of sexual behavior.

Recessive *Pclo* traits are mappable to allelic markers for major depressive disorder

Mapping to a recessive phenotype, the *Synaptic Transmission* category included a severely compromised *Glutamatergic Excitation* gene set (GO:0051966, p=0.00000001) in the brain of homozygous animals (e.g. DEGs in the *Pclo^{gt/gt}*, but not in *Pclo^{gt/wt}* mutants) (Supplementary Table 6). Among the most significantly downregulated genes were *Grm5* (top 20) (Glutamate Metabotropic Receptor 5) and *Htr2a* (the serotonin [5-Hydroxytryptamine] Receptor 2A) (Supplementary Table 5). Both *Grm5* and *Htr2a* function as GPCRs in the signaling cascade that controls calcium mobilization and PKC activation^{39, 40}. Alongside *glutamatergic* neurotransmission, *dopaminergic* neurotransmission (e.g. *Drd2*) and *neuronal Calcium signaling* (e.g. *Cacna2D1*) also contribute to the recessive phenotype of *Pclo* mutations.

Intriguingly, *Pclo*, *Grm5*, *Htr2a* and *Drd2* are among 44 genes that have recently been reported as key risk factors of major depressive disorder (MDD), supported by independent (including a >135K) GWASs on human patients with MDD (Fig. 6a)^{41, 42}. To test a potential relationship between Piccolo and depression, we data-mined and compared the

transcriptome of an MDD rat model⁴³ to the transcriptome of our *Pclo*-KO rat brain. Our strategy identified a robust list of 408 genes that were similarly affected in both models ($rho = 0.306$ and $p\text{-value} = 2.916e-08$) (Fig. 6b), supporting a transcriptome-level relationship between the biological processes dysregulated in *Pclo*-KO and neurological disorders categorized as MDD. Notably, the shared list of Major Depressive disorder includes genes such as *Plac8* and *Ift1* that have been associated with various features of depression, such as fear (e.g. *Hsbp1*), cortical dementia (e.g. *Trim47*), moodiness (e.g. *S100A9*) or depression followed by immune challenge (e.g. (Fig. 6c)). Interestingly, *Gabra6*, which was among the most highly dysregulated genes in *Pclo* KO, is also not detectable in the MDD hypothalamus (Fig. 6d).

Reproductive failure in *Pclo* mutant rats is associated with behavioral defects

Following up on the neurotransmission and reproduction phenotypes observed in the *Pclo* mutants, we conducted further studies on brain functions and behavior. Consistent with a dominant phenotype (Supplementary Fig. 5), both *Pclo*^{wt/gt} and *Pclo*^{gt/gt} mutations increased the occurrence of mean seizure frequencies (≥ 8 -fold) compared to *Pclo*^{wt/wt} littermates ($n=8/\text{genotype}$) (Fig. 7a, top). The EEG morphology in *Pclo*^{wt/gt} and *Pclo*^{gt/gt} rats was consistent with short duration, absence-type seizures, displaying a characteristic 6-8 Hz spike-wave generalized onset (Fig. 7a, bottom), with no convulsive activity, and functionally verifying significance of altered *Synaptic Transmission* gene sets (Fig. 5a, b; Supplementary Fig. 5, Supplementary Table 6).

Pclo^{wt/wt} and *Pclo*^{wt/gt} rats of the opposite or same sex displayed typical social behavior upon being introduced into the same cage (Supplementary Video 1-4). In contrast, *Pclo*^{gt/gt} rats

exhibited a relative disinterest in the opposite sex in the same test with *Pclo*^{wt/wt} or *Pclo*^{wt/gt} rats (p=0.0002 compared to WT littermates, n=8/genotype) (Supplementary Video 5-7). Instinctive, pre-copulatory social interactions such as courtship, grooming, and genital investigation that normally occur between female and male rats were not observed in *Pclo*^{gt/gt} rats of either sex (Supplementary Videos 5-7). The mating disorder phenotype of *Pclo*^{gt/gt} rats of both sexes (Fig. 4b) included abnormal conspecific social behavior, displaying overt aggression, biting or defensive lunging/posturing (Fig. 7b, Supplementary videos 5-7).

Cross-species analysis reveals robust differences in rat reproduction mutant phenotypes

We compared our phenotypes in rats to mutant phenotypes recorded in other species harboring loss-of-function mutations in orthologous genes (Supplementary Table 4). Nine mutated rat genes (*Atg13*, *Btrc*, *Dlg1*, *Grik3*, *Pclo*, *Slc1a3*, *Spaca6*, *Zmynd8*, and *Ube2k*) have mutated orthologs in mice (Mouse Genome Informatics (MGI), the International Mouse Phenotype Consortium (IMPC) and the National Center for Biological Information (NCBI) databases), while 5 of our mutated orthologs have been characterized in plants, yeast, worms, flies or frogs (i.e. *Alk3*, *Atg13*, *Btrc*, *Dlg1*, *Pan3*) (Supplementary Table 4).

In humans, genome-wide association studies (GWAS) have implicated orthologs for 12 of the mutant rat genes we analyzed (*Abca13*, *Alk3*, *Atg13*, *Btrc*, *Dlg1*, *Exoc6b*, *Fstl5*, *Gsgl1*, *Grik3*, *Pclo*, *Slc1a3*, *Ube2q2*) as either risk factors or candidate risk factors for various human disease processes, curiously about half of them (e. g. *Abca13*, *Dlg1*, *Exoc6b*, *Grik3*, *Pclo*, *Slc1a3*) with neurological/behavioral disorders (Supplementary Table 4). Strikingly, the ‘shortened life span’ caused by mutations in *Atg13* has been reported across multiple species

including plants, yeast, worms, flies, mice and rats (Supplementary Table 4). In *ATG13*^{gt/gt} rats, a shortened life span was uniquely mapped to a carboxyl-terminal polypeptide in WT *ATG13* (Fig. 3).

Our comparative analysis provided several examples in which mutations in genes in the rat strains analyzed here and their orthologs in another species produced significantly different phenotypes (Supplementary Table 4). These differences may reflect the quality of the knockout and/or species-specific differences in biology. While reproduction and behavior is normal in mice that have been designed to model human *Pclo* variants,⁴⁴ our approach revealed phenotypes in rats consistent with defects in humans (Supplementary Table 4) and allowed us to discover a genetic link between *Pclo*, reproductive failure and CNS disorders.

Discussion

Here we characterize a pool of 12 pre-selected mutant rat strains from a forward genetic screen for reproductive phenotypes. The mutant rat strain pool was derived from a recombinant spermatogonial library of *Sleeping Beauty* genetraps insertions¹². The mutant genes transmitted an inability of rats to reproduce (*Alk3*, *Atg13*, *Dlg1*, *Btrc*, *Exoc6b*, *Pan3*, *Pclo*, *Slc1a3*, *Spaca6*, *Tmx4*, *Ube2k*, *Zmynd8*). The reproduction phenotypes we identified were all associated with different steps in spermatogenesis or embryonic lethality with the exception of three mutant strains (*Atg13*, *Dlg1*, *Pclo*). In those cases, *Atg13* and *Piccolo* strains stood out by exhibiting a “complex” phenotype that allowed us to decipher novel aspects of reproduction. Importantly, *Atg13* and *Piccolo* mutations are also phenotypically related to clinically relevant metabolic and neurological disorders in humans.

Our *Atg13*^{gt/gt} rats displayed abnormal autophagy markers, gross renal abnormalities and inflammation-like phenotypes that preceded death in early adulthood. ATG13 (Autophagy related 13) is the master metabolic sensor for toggling between AMPK1-dependent cellular torpor (i.e. autophagy) and ULK1-repressed mTORC1-dependent cell growth. The *Atg13*^{gt/gt} rat phenotype might be related to the loss of a phylogenetically conserved Ulk1-binding peptide encoded by the *Atg13*'s terminal exon (Fig. 3), implicated in activating the main autophagy-initiating complex⁴⁵. Similar to the rat *Atg13*^{gt/gt} phenotype, dysfunctions in *Atg13* have been associated with nephrological and immunological problems and autophagy in humans⁴⁶⁻⁴⁸. Mice harboring either a frameshift mutation in *Atg13* exon 5 or a genetraps in *Atg13* exon 1, by contrast, exhibit a more severe phenotype and die *in utero* due to heart defects⁴⁹. Notably, the end-stage pathology of *Atg13*^{gt/gt} rats correlated with immotile,

degenerating caudal epididymal spermatozoa, likely associated with the premature aging phenotype.

While the *Atg13^{gt/gt}* rat represents an excellent model to study the connection between premature aging, fitness and fertility, our *Pclo* mutant highlighted how traits linked to human neurological disorders may disrupt rodent reproductive behavior. Curiously, the *Pclo*^{SBA4-25} mutation results in infertility, but induces more robust “global” changes in the brain transcriptome than in the testis, suggesting a possible crosstalk between the brain and gonads. The most significant changes in both tissues affected GABAergic signaling, in particular, through GABA(A) receptors.

GABAergic signaling could connect brain and testis in multiple ways. First, GABA(A) receptors are implicated in the maturation of GnRH neurons in the brain (e.g. *Gabra6*)³². Although *Gabra6* was severely affected in *Pclo* mutants, our *in situ* staining performed on the pre-optic area of the hypothalamus detected no deviation in their number or distribution from the wt, arguing against the GnRH maturation hypothesis. Our data are more supportive of a second scenario in which the infertility phenotype is connected to the Piccolo-dependent dysfunctions in GABAergic synaptic transmission (Fig. 5a, b) and GnRH pathways (Supplementary Figs. 6, 7) is reminiscent of the long-standing debate regarding the manner in which GABAergic tone in the brain and testes is functionally linked to circulating and/or locally produced gonadotrophins⁵⁰. In *Pclo*^{SBA4-25} rat testes, endophenotypes may also predict a compromised role of GABA(A) receptors in triggering spermatozoa activation^{51,52}, whereas, crosstalk between brain and testes is possible *via* a common mechanism that

normally maintains GABAergic tone. Importantly, disturbed *GABAergic synaptic transmission* in *Pclo* mutants likely affects the balance between inhibition and excitation and thereby provokes seizures⁵³, which manifests itself as epileptiform activity.

As is the case with knockouts of *Pclo*, mutations in *Gabra6* also cause generalized seizures in human patients⁵⁴⁻⁵⁷ and exhibit expression levels close to KO phenotype in an MDD rat model⁵⁸. The functional significance of the tight control of *Gabra6* expression by *Pclo* has yet to be investigated, but one possibility is that a loss of synaptic integrity leads to its down-regulation⁵⁹. Even so, reports on *Gabra6* KO mice suggest that they exhibit no behavioral phenotypes⁶⁰⁻⁶², suggesting that the complexity of the phenotypes observed in *Pclo*^{gt/gt} rats may not be entirely explained by *Gabra6*-deficiency alone. It is interesting to note that the dysregulation of the testis-predominant *Gabrg3* is associated with alcoholism⁶³⁻⁶⁵, epilepsy⁶⁶ and autism spectrum disorder^{67, 68}.

Patients homozygous for a frameshift mutation that introduces a STOP codon in *Pclo* exon 6 (*Pclo*^{e6-stop}) inherit *pontocerebellar hypoplasia type 3a*¹³. Adolescents homozygous for *Pclo*^{e6-stop} display optic, cerebral, cerebellar and spinal atrophy with reduced white matter volume, while children develop generalized seizures similar to those observed in our *Pclo* mutant rats (Fig. 7a)¹³. *Pclo* mutations have further been classified in association with a high risk for abnormal emotional processing, independent of executive functions⁶⁹. Patients with *Pclo* mutations display blunted emotional responses to fearful or angry faces that correlate directly with enhanced regional brain activity in the amygdala⁶⁹. Thus, the affective disorder and limbic system neurotransmission phenotypes observed in patients^{69, 70} are consistent

with an essential role for *Piccolo* in normal conspecific social behavior in rats (Fig. 4b, Fig. 7b, Supplementary videos 1-7).

Nevertheless, while human *Piccolo* variants are clearly associated with neuronal phenotypes, no direct sexual connection has been reported to date⁷¹. In *Pclo*^{SBA4-25} rats, by contrast, the failure to reproduce suggests a scenario consistent with a disrupted reproductive behavioral phenotype. The rodent limbic nervous system controls a hierarchy of brain centers orchestrating the sequential steps of reproduction behavior. This process plays an important role in male-specific patterning in the hypothalamus, and its disruption leads to disturbed sexual behavior, including aggression and anxiety phenotypes²⁻⁴. The lack of pre-copulatory, copulatory behavior and the enhanced aggressive behavior in either sex of *Pclo*^{gt/gt} rats (Supplementary Videos 1-7) might be associated with compromised synaptic transmission in the olfactory and/or limbic system, (and perhaps the hypothalamus; Fig. 7c)^{3, 4}. The hypothalamus is innervated by the amygdala and the bed nucleus of the stria terminalis (BNST) and is responsive to modulation by sex hormones (estrogen, testosterone); these neural connections are associated with downstream pre-copulatory (lordosis), copulatory (mounting, intromission, ejaculation) and post-copulatory (parental care) reproductive behaviors (Fig. 7c)^{3, 4}.

Down-regulated sets of *Hormonal Secretion* and *Response* genes in the *Pclo* rat brain (Fig. 5b) may induce compensatory responses. Such a reciprocal relationship may reflect the upregulation of the “anti-stress” neuropeptide Y (*Npy*) in *Pclo*^{gt/wt} and *Pclo*^{gt/gt} rat brains (Fig. 4f, Supplementary Table 5). An exposure to an overdose of *Npy* inhibits sexual behavior in normal rats⁷². Curiously, intracerebroventricular applications of *Npy* in the OBx depression

rat model with mating disorders^{38, 38, 73} elicited anti-depressive affects, whereas Npy Y1 receptor antagonists stimulated depression phenotypes^{74, 75}. Thus, Npy may link sexual behavior and depression phenotypes via neuroendocrine secretions. Still, despite studies identifying associations between human sexual motivation and depression⁷⁶, a clear relationship between gene mutations that link depression to repressed sexual behavior in humans has not been clearly established.

Importantly, a clear association between *Pclo* mutations and depressive phenotypes is supported by a related transcriptome of an MDD rat model and our homozygous *Pclo* rat brain (Fig. 6). Intriguingly, the list of genes dysregulated by allelic gene expression in *Pclo* rats matches the list of key allelic neurological markers for MDD in human patients^{15-17, 41}. Indeed, other than *Pclo*, the major risk factors for MDD (e.g. *Grm5*, *Htr2a*, *Sorcs3*, *Negr1*, *Drd2*) were recently identified independently in large scale GWAS cohorts diagnosed with bipolar¹⁴ and major depressive disorders (MDD)^{15-17, 41}.

In contrast to the neurological disease states caused by *Pclo* variants in humans¹³⁻¹⁷ and rats (Figs. 4-7), mice harboring the most widely studied *Pclo* variant implicated in depression, rs252283 (Ala-4814-Ser), or mice that lack the full calcium sensing coil-coil domain mutated by rs252283, behave normally^{77,44}. This suggests that the *Pclo*^{SBΔ4-25} rat appears to more faithfully model certain types of human neurological/behavioral diseases, including MDD.

Our work highlights the potential to be gained by expanding research on disease-related genes to alternative model organisms at a time when diverse genome editing technologies are revolutionizing genome manipulation. Our screen demonstrates the power of unbiased

random *Sleeping Beauty* transposon mutagenesis to identify unanticipated functions for reproduction genes in neurobiology and other critical processes. Such unusual gene-function associations might easily have been missed by a candidate approach using targeted mutagenesis. The phenotypical diversity observed within the small sample of spermatogonia-derived mutant rats underscores the robustness of our forward genetic approach (Fig. 1). Notably, knockdown strategies would not be suitable to track allelic regulation. Performing the screen in rats has proven to be strategically important, considering the complex behavioral relationships revealed by the Piccolo mutant.

Online Methods

Mutant rat strains

Mutant rat strains harbored *Sleeping Beauty* β -*Geo* trap transposons⁷⁸ originally transmitted from a donor, recombinant rat spermatogonial stem cell library¹². Recipient males were bred with wildtype females to produce a random panel of mutant rat strains enriched with genetraps in protein coding genes¹². Eighteen mutant rat strains were evaluated in the current study (Supplementary Tables 1 and 2). Rat protocols were approved by the Institutional Animal Care and Use Committee (IACUC) at UT-Southwestern Medical Center in Dallas, as certified by the Association for Assessment and Accreditation of Laboratory Animal Care International (AALAC).

Genotyping mutant rat progeny

Endogenous gene-specific PCR primers near *Sleeping Beauty* integration sites were used in combination with transposon-specific primers to genotype progeny from familial generations F1 and F2 for newly generated mutant rat lines. Genomic sites of transposon integration were defined in F1 progeny by splinkerette PCR¹² and sequence analysis alignment on genome build RGSC v3.4 (Rn4). Genotyping results were verified by Southern blot hybridization assays of genomic DNA digested with XmnI and XbaI using a probe specific for the *EGFP* transgene and the *LacZ* portion of the β -*Geo* insert in the *Sleeping Beauty* transposon¹². Restriction analysis by Southern blot estimated ~7 transposon integrations/stem cell genome, which following random segregation and ploidy reduction during meiosis yielded ~3.5 transposon integrations/donor-derived spermatozoa, or founder-derived mutant F1 pup¹². Phenotypes in *Atg13*, *Btrc*, *Pclo*, *Pan3*, *Spaca6* and *Ube2k* *Sleeping Beauty* mutant rat strains were analyzed in F4 animals produced from F3 breeder

pairs harboring only their respective, *Sleeping Beauty* transposon integration (i.e. single copy gene-trap transposon F3 mutants).

Rat breeding for forward screen

Founder-derived F1 mutant progeny were crossed with wildtype rats to produce F2 mutants. Males and females for 17 of 18 F2 heterozygous mutant strains successfully produced litters, of which, mean litter sizes produced by 15 of the F2 heterozygous mutant strains were comparable in size to wildtype Harlan, Sprague Dawley rat stocks (Supplementary Table 2). Only *Dlg1*^{wt/gt} females were identified as sub-fertile after pairing heterozygotes with wildtype rats of opposite sex for >10 months. One *Dlg1*^{wt/gt} female produced a single mutant female from one litter (n=4 pups); however, the second generation *Dlg1*^{wt/gt} female failed to reproduce after subsequent pairings with fertile males for 12 months. Male and female (F3) heterozygous mutants from the other 17 strains were generated from separately outbred parents (Harlan, SD) and paired at 3-4 months of age to generate F4 homozygous mutants. Heterozygous mutant pairs that produced litters and displayed markedly reduced Mendelian rates towards generation of homozygous mutant progeny were classified as embryonic lethal (i.e. no homozygous mutant F4 progeny; n>50 total pups/strain except for *Alk3*^{wt/gt} mutants, where n=35). Viable F4 homozygous mutants were paired with proven wildtype breeders (Harlan, SD) of opposite sex between 3-4 months of age to identify recessive mutations that transmitted significant changes in mean litter size. If F4 homozygotes failed to generate progeny by 3-4 months after pairing with a wildtype breeder, they were paired with a second wildtype proven breeder from Harlan, SD. Genes were classified as required for rat reproductive success under our standard housing conditions if homozygous mutations blocked multiple F4 progeny (n=2-4 homozygous

mutant breeders/sex) from producing any offspring after pairing with 2 consecutive wildtype proven breeders of similar age over a span of >10 months. Adult lethal homozygous *Atg13* mutants demonstrated health decline between 3-4 months of age (i.e. shortly after setting up breeder pairs).

Phenotype database and literature analysis

European Conditional Mouse Mutagenesis Programme (EUCOMM), Knockout Mouse Project (KOMP), Mouse Genome Informatics (MGI), International Mouse Phenotype Consortium (IMPC) and National Center for Biological Information (NCBI) databases provided records on mouse gene orthologs. NCBI PubMed, Gene and the Rat Genome Database (RGD) provided records on rat gene orthologs. Human phenotypes for mutant orthologs were searched in publically available NCBI Genetics and Medicine databases, including: PubMed, Gene, Online Mendelian Inheritance in Man (OMIM), Database of Genotypes and Phenotypes (dbGaP); and the National Human Genome Research Institute's Catalog of Published Genome Wide Association Studies (NHGRI GWAS Catalog). NCBI PubMed and Gene were searched to identify phenotypes available for *Arabidopsis*, *Saccharomyces*, *Caenorhabditis*, *Drosophila*, *Danio* and *Xenopus* species. PhenomicDB database verified results from above database searches across all species. Literature comparisons for phenotypes caused by mutations in rat and mouse orthologs published independent of the current study are summarized in Supplementary Table 4. Embryonic lethality or postnatal lethality prior to reproductive age was categorized as blocking reproduction. Fishers Exact t-test (two-tailed) was used to analyze phenotypic proportions of viable versus sub-viable, viable versus embryonic lethal, fertile versus infertile, mating versus non-mating.

Electroencephalogram (EEG) recording and analysis

Twelve adult rats (6 male, 6 female) were surgically prepared for EEG experiments with 4 rats in each experimental group (*Pclo*^{wt/wt}, *Pclo*^{wt/gt}, *Pclo*^{gt/gt}). Rats were anesthetized using a gas anesthesia machine with ~3% isoflurane in a 1 L/min mixture of 70% nitrous oxide and 30% oxygen. Four epidural recording electrodes made from #00-90 x 1/8 inch stainless steel screws were placed at the following stereotaxic coordinates: A-P \pm 2.0 mm, lateral \pm 3.0 mm and A-P - 4.0 mm, lateral \pm 3.0 mm along with a reference and ground screw over the olfactory bulb and cerebellum, respectively. Electrodes were attached by a flexible wire (kynar, 30 ga) to a custom 6-pin micro-connector (Omnetics) and secured with dental acrylic. Rats received the analgesic buprenorphine (0.05 mg/kg) as necessary following surgery and were allowed to recover for at least 7 days prior to any experimentation. Following recovery from electrode implantation, each rat was placed in a custom acrylic recording cage (Marsh Designs, Peoria, AZ) and connected to a Tucker-Davis Technologies (Alachua, FL) RZ2/PZ3 neurophysiology workstation through a flexible cable suspended from the top of the cage with an interposed commutator to allow rats free access to food and water without twisting the cable. Continuous video/EEG (300 Hz sampling) was recorded for each rat simultaneously for 7 days and read by a user blinded to the experimental grouping for the presence of seizures and epileptiform activity. Seizure activity was marked at the beginning and end of each event to account for seizure duration, and the numbers of seizures per hour were calculated.

Western blot analysis

To analyze Piccolo expression, brains were dissected from wildtype, heterozygous mutant, and homozygous mutant Sprague Dawley rats and homogenized in 1.5 ml/0.5g tissue, ice-

cold lysis buffer (50 mM HEPES, pH 8.0, 150 mM NaCl, 1 mM EDTA, 10% glycerol, 1% Triton X-100, 10 µg/ml aprotinin, 10 µg/ml leupeptin and 1 protease inhibitor tablet/12.5 ml) for 30s using a PTA-7 probe, setting 5, PT10-35 polytron (Kinematica). The homogenates were incubated on ice for 15–20 min and then centrifuged at 3000 xg for 10 min at 4°C in a GPR tabletop centrifuge (Beckman, Inc.). The supernatant solutions were centrifuged at 15,800 xg for 15 min at 4°C in a microcentrifuge (Model 5042, Eppendorf, Inc.) and the resultant supernatant fractions were stored at -80°C. 160 µg of protein was separated on 4-15% Mini-Protean TGX gels (BioRad, Inc.), and then transferred to nitrocellulose. Samples were not heated prior to loading. Nonspecific, protein binding sites were blocked by incubating membranes overnight at 4°C in blocking buffer: TBST (Tris-buffered saline with Tween-20: 10 mM Tris-HCl, pH 7.5, 150 mM NaCl, 0.1% Tween-20) containing 5% nonfat dry milk. Membranes were washed three times in TBST and incubated for 1 h at 22–24°C using rabbit anti-Piccolo (Synaptic Systems cat. no. 142002) diluted 1:2000 in blocking buffer. Membranes were washed three times in TBST (0.3% Tween-20) and incubated 45 min, 22–24°C with peroxidase-conjugated, anti-rabbit IgG (Jackson Immunoresearch) diluted 1:50,000 in blocking buffer. Membranes were washed three times in TBST and protein bands detected using the enhanced chemiluminescence detection method (ECL, Amersham, Inc.). Blots were stripped and re-probed with 1:20,000 dilution of mouse anti-TUBA1a (MU-121-UC, Biogenex, Inc.).

Rat embryonic fibroblast (REF) cultures were extracted in RIPA buffer (50 mM Tris pH 7.4, 150 mM sodium chloride, 1 mM EDTA, 1% IPEGAL, 0.25% deoxycholic acid) plus protease inhibitor and phosphatase inhibitor tablets (Roche Applied Science). 11 µg protein was separated on NuPAGE 4-12% Bis-Tris gels (Invitrogen, Inc.) and then transferred to

nitrocellulose membranes. Nonspecific protein binding sites were blocked by incubating membranes overnight at 4°C in blocking buffer: TBS (Tris-buffered saline: 10 mM Tris-HCl, pH 7.4, 150 mM NaCl) containing 1X Western Blocking Reagent (Roche Applied Science, Inc.). Antibodies were diluted in TBS containing 0.5X Western Blocking Reagent + 0.1% Tween-20. Membranes were incubated in primary antibody for 1-2 hours at 22-24°C. Membranes were washed 4 x 5 min in TBST (0.1%-0.3% Tween-20), incubated in IRDye secondary antibody for 45-60 min, washed again 4 x 5 min, and scanned on an Odyssey Classic Quantitative Fluorescence Imaging System, Model 9120, Licor Biosciences, Inc. Images were analyzed with Odyssey software version 3.0.21. Primary antibodies: Rabbit anti-LC3A from Cell Signaling Technology, Inc, #4599, 1:300; Mouse anti-ATG13 from Medical and Biological Laboratories, Ltd, #M183-3, 1:1000; Guinea pig Anti-p62 from Medical and Biological Laboratories, Ltd, #PM066., 1:2000. Secondary antibodies were all from Licor Biosciences: Goat anti-rabbit IRDye 800CW #926-32211, 1:15000; Goat anti-mouse IRdye 680LT 1:20000; Donkey anti-guinea pig IRDye 800CW #926-32411, 1:15000.

Sperm counts and copulation

Epididymides were harvested from adult rats between 120-180 days of age and dissected free of surrounding fat and connective tissue for measuring weights, counting spermatozoa and histological analysis. To estimate spermatozoa numbers/rat, each epididymal caput and cauda were dissected apart from the corpus and separately placed into 3.8 cm² wells of a 12 well plate containing 1.5 ml DHF12 nutrient media [Dulbecco's Modified Eagles Medium:Ham's F12 (1:1); Sigma, D8437] 1x antibiotic antimycotic solution (Invitrogen, cat. no. 15240-062). Spermatozoa were released by thoroughly mincing each epididymal piece for 30 sec and allowing the spermatozoa to disperse into the medium for 25 min. Large

pieces of epididymal tissue were removed with forceps and discarded. One ml of the epididymal cell-containing medium was carefully filtered through a 100 μ m cell strainer (BD Biosciences, Inc.) into a 1.5 ml microfuge tube prior to counting using a Hemocytometer chamber. To assess breeding behavior and detect copulation, rats were paired with a single wildtype mate just prior to the end of the daily light cycle (4:00-5:00 pm central standard time). The following morning (7:00-8:00 am central standard time), each female was examined for the presence of spermatozoa in the vagina. A foam swab tip was used to collect a vaginal smear, which was then analyzed by phase contrast microscopy to detect presence of sperm.

Rat embryonic fibroblast culture

Primary rat embryonic fibroblast (REF) cultures were prepared from E14.5 embryos dissected from wildtype female rats after mating with *Atg13*^{wt/gt} male rats. Timed mating was established as described above in the section on *Sperm Counts and Copulation*. Uteri were dissected from pregnant females and washed with 10 ml DHF12 medium, 1% Penicillin-Streptomycin solution (v/v). The heads and visceral tissue were removed from each isolated embryo. Visceral tissue was discarded. Tissue from the upper portion of the head was used to isolate genomic DNA and genotype embryos for the *Atg13* genetrapped mutation. The remaining thoracic portion was washed in fresh DHF12 medium, transferred into tubes containing 5 ml 0.05% trypsin/1mM EDTA solution, minced for 2 minutes and then incubated at 37°C for 20 min. After incubation, REF culture medium [DMEM (Sigma, D5648-10XL), 10% fetal bovine serum (Tissue Culture Biologicals, 104300), 1% Penicillin/Streptomycin (Hyclone, SV30010)] was added to the cell suspension and the cells were dissociated further by gentle trituration (5 strokes) using a p1000 Eppendorf tip. The

cell suspension was centrifuged 4 min at 120 x *g* and the supernatant was discarded. The cellular pellet was retained, suspended to 15 ml in fresh REF medium, plated into 10cm plastic tissue culture dishes (Corning, Inc.) and then incubated at 37°C, 5% CO₂ overnight. REFs were fed 15 ml fresh medium every 48 hrs, and sub-cultured using the 0.05% trypsin/1mM EDTA solution to harvest attached cells from culture dishes every 2-3 days. Harvested REFs were passaged by plating at ~10⁴ cells/cm² in 3 ml/cm² REF medium. REF cultures were maintained at 37°C, 5% CO₂, and used for experiments at passage 4. REFs were treated for 24 hr with or without 3 mM ammonium chloride (Fluka, 09718), 100 nM Rapamycin A (LC Laboratories, R-5000) and, or 3 nM Bafilomycin A1 (Sigma, B1793) prior to preparing lysates for western blots.

Histological sectioning and staining

Hematoxylin/Eosin (H&E), periodic acid-Schiff's (PAS) and Trichrome staining on histological sections from rat tissues were conducted by standard procedures at the Molecular Pathology Core Laboratory, UT Southwestern Medical Center in Dallas.

Preparing frozen sections

To prepare frozen testis sections for labeling with antibodies, testes were dissected from rats, perforated by puncturing three equally spaced holes in the *tunica albuginea* along each longitudinal axis of the testis using a 27 gauge needle, and fixed for ~18 hr at 4°C in 0.1M sodium phosphate buffer, pH 7.2, containing 4% paraformaldehyde. Fixed testes were equilibrated through a 10%, 18% and 25% sucrose [wt/v, dissolved in 1x phosphate buffered saline (PBS; Invitrogen Inc, cat no. 14040-182)] gradient by sequential overnight incubations (~24 hr) at 4°C in 20 ml of each respective sucrose solution. Once equilibrated

to 25% sucrose, testes were embedded in tissue freezing medium (Electron Microscopy Sciences Inc., #72592) and frozen using a Shandon Lipshaw (#45972) cryo-bath. Frozen testes were used to prepare a parallel series of 8 μm cryo-sections. Frozen sections were stored at -40°C until use in immunofluorescence assays as described below.

Fluorescence immunohistochemistry

Prior to labeling studies, sections were equilibrated in air to $\sim 22\text{-}24^{\circ}\text{C}$ for 15 min, hydrated in Dulbecco's phosphate-buffered saline (PBS) (Sigma, D8537) at $22\text{-}24^{\circ}\text{C}$ for 10 min, heat-treated at 80°C for 8 minutes in 10 mM sodium citrate (pH 6.0) and then incubated for 1 hr at $22\text{-}24^{\circ}\text{C}$ in blocking buffer [Roche Blocking Reagent (1% v/v) diluted in 0.1M Sodium phosphate buffer, containing Triton X100 (0.1% v/v)]. Sections were then treated for 18-24 hr at $22\text{-}24^{\circ}\text{C}$ with respective antibodies diluted in blocking buffer at the following concentrations: [1:400 mouse anti-Sall4 IgG (H00057167-M03, Abnova, Inc); 1:400 rabbit anti-phospho-H2A.X (Ser139) IgG (07-164, Millipore, Inc); 1:400 rabbit anti-phospho-Histone H3 (ser10) IgG (06-570, Millipore, Inc)] diluted into Roche blocking (1% w/v) reagent. After treatment with primary antibodies, sections were washed 3 times for 10 min/wash in 50 ml PBS and then incubated for 40 min at $22\text{-}24^{\circ}\text{C}$ with respective AlexaFluor594 (Invitrogen, Inc), or AlexaFluor488 (Invitrogen, Inc) secondary antibodies diluted to 4 $\mu\text{g}/\text{ml}$ in PBS containing 5 $\mu\text{g}/\text{ml}$ Hoechst 33342 dye (Molecular probes, cat no. H3570). After treatment with secondary antibodies, sections were washed 3 times at 10 min/wash in 50 ml PBS. After the 3rd wash in PBS, sections were cover-slipped for viewing using Fluorogel mounting medium (Electron Microscopy sciences, cat no. 17985-10). Images were acquired using an IX70 Olympus fluorescence microscope (Olympus Inc.)

equipped with Simple-PCI imaging software (C-Imaging Systems, Compix, Cranberry Township, PA).

Perfusion, Sectioning and Immunohistochemistry of rat brains

Perfusion: Adult rats (P100) were first sedated in Isoflurane (Abbott GmbH & Co. KG, Wiesbaden, Germany) and then deeply anesthetized with a mix of 20 mg/ml Xylavet (CO-pharma, Burgdorf, Germany), 100 mg/ml Ketamin (Inresa Arzneimittel GmbH, Freiburg, Germany) in 0.9% NaCl (B/BRAUN, Melsungen, Germany). Afterwards the heart was made accessible by opening the thoracic cavity, and a needle inserted into the left ventricle and the atrium cut open with a small scissor. Animals were initially perfused with PBS and then with freshly made 4 % PFA, before dissected and further for 24h incubated in 4 % PFA at 4°C. Subsequently the brains were cryoprotected in 15 % and then 30 % sucrose at 4°C for 24h each. Brains were then frozen using 2-methylbutane (#3927.1, Carl-Roth, Karlsruhe, Germany) cooled with dry ice to -50°C and stored at -20°C.

Brain sectioning. 20 µm thin serial sections were cut from frozen brains using a cryostat (Leica Mikrosysteme Vertrieb GmbH, Wetzlar, Germany). Slices transferred to a microscope slide (Superfrost Plus, #H867.1, Gerhard Menzel B.V. & Co. KG, Braunschweig, Germany), dried at RT for at least 1h and stored at -20°C.

Immunohistochemistry. 3,3'-Diaminobenzidine (DAB) staining of 20 µm coronal brain sections labeled with mouse anti GnRH antibody performed as previous described (Brinschwitz et al., 2010). In brief, thawed sections were dried for 30 min at RT and washed 3x for 10 min in PBS-T (PBS 1X (Thermo Fisher Scientific, Waltham, USA) + 0.025% Triton X-100 (#3051.2, Carl-Roth, Karlsruhe, Germany) and endogenous peroxidase was blocked for 10 min with 0.3% H₂O₂ in PBS, before blocking for 2h at RT in blocking solution (PBS

plus 10% normal goat serum and 1% BSA). Sections were then incubated in primary mouse anti GnRH antibody (1:500, HU4H, provided by H. Urbanski, Oregon Regional Primary Center, Beaverton, OR) in blocking solution for 1h at RT and 2 days at 4°C. After washing sections were incubated in a secondary Biotin-conjugated antibody (goat anti mouse Biotin-SP, 1:1000, #115-035-003, Dianova GmbH, Hamburg, Germany) in blocking solution for 1h at RT and 2 days at 4°C, before adding the ABC reaction reagent (Vectastain ABC Kit #PK-6100, Vector Laboratories Inc., Burlingame, CA) for 1h at RT and 1 day at 4°C. After 1 day, sections were washed before adding the DAB solution (DAB peroxidase substrate Kit #SK-4100, Vector Laboratories Inc., Burlingame, CA) for 1min. DAB reaction was stopped with purified water (ddH₂O) and sections were dehydrated in the following sequence: 2 min 70 % ethanol (EtOH), 2 min 80 % EtOH, 2 min 95 % EtOH, 2 min 99,9% EtOH. Sections were cleared in Rotihistol (#6640.4, Carl Roth GmbH, Karlsruhe, Germany) until mounting in Entellan (#1.07961.0100, Merck KGaA, Darmstadt, Germany).

Analysis of RNA-seq data from Pclo rats

Single end 100 bp RNA-seq libraries were prepared from brain, liver and testis tissues of ~6-month-old Pclo^{gt/gt}, Pclo^{gt/wt}, Pclo^{wt/wt} rats. The libraries were run on *Illumina Hiseq 2000* sequencer (Total number of reads was ~550-600 million). For *basecalling* we used the *Illumina Casava1.7* software. Reads were then aligned to the reference human genome version *rn6* by using *Tophat2/bowtie2*. This approach has provided a *refseq_rn6* gene model that guided the assembly process of the transcriptome. We checked the quality of the sequencing and the mapping by *Fastqc* and by *RNASeqQC*, respectively. Due to the negligible technical variances, the read counts of a gene had a Poisson distribution⁷⁹, thus we could apply the single-replicate model to analyze the data. We calculated Read counts using

featureCounts from the *subread* package (<http://subread.sourceforge.net/>). FPKM was calculated using *bamutils* (<http://ngsutils.org/modules/bamutils/count/>).

Analysis of differentially expressed genes

Random Variable1 ($Var1$) = $n.l.x$, where x (Random Variable2) is the expression level of a gene (e.g., in RPKM (Reads Per Kilo bases per Million reads)⁸⁰, n is reflecting the sequencing depth and l is the gene length. The method proposed by Anders and Huber was used to calculate n ⁸¹. To generate more robust and accurate *Fold change* values from unreplicated RNA-seq data, we determined the normalization constant and variance by pasting the two random variables in the published algorithm of:

<http://bioinformatics.oxfordjournals.org/content/early/2012/08/23/bioinformatics.bts515.full.pdf+html>). To identify the Gene Ontology (GO) categories that were overrepresented in the Piccolo mutants, we compared samples from the brain and testis of *Pclo*^{gt/gt} and *Pclo*^{wt/gt} vs *Pclo*^{wt/wt} rats, with the entire set of rat genes as a background.

Acknowledgments

This work was supported by National Institutes of Health grants to F.K.H. from The Eunice Kennedy Shriver National Institute of Child Health and Human Development: R01HD053889 and R01HD061575, The National Center for Research Resources: R24RR03232601; and The Office of the Director: R24OD011108. Neurological analyses on *Pclo* mutant rats were conducted by The Neuro-Models Facility (EJP, LBG) at UT Southwestern Medical Center, and supported by the Haggerty Center for Brain Injury and Repair. Z. Iv. was supported by grants from the Bundesministerium für Bildung und Forschung (NGFN-2, NGFNplus - ENGINE). Z. Iz. is supported by European Research Council, ERC Advanced [ERC-2011-AdG 294742]. CG is supported by the German Center for Neurodegenerative Diseases (DZNE) and DFG-SFB958. We thank Christine Römer and Ruth Ann Word for their critical comments.

Figure Legends

Fig. 1. Spermatogonia-Mediated Forward Screen for Rat Reproduction Genes

Recombinant rat spermatogonial stem cell libraries are produced by *Sleeping Beauty* transposon genomic insertion. Spermatogonial cultures harboring random *Sleeping Beauty* genetraps are used to produce colonies of mutant rats. Novel *Sleeping Beauty* mutant rat strains are crossed to study reproduction phenotypes. In the current study, twelve homozygous mutant rat strains generated were viable following birth (~70%), 5 were embryonic lethal (~28%), and 1 was scored as sub-viable postnatally (~6%) (n=18 mutant rat strains analyzed for ability to reproduce). Mutation induced embryonic lethality and sub-viability rates in rats measured in the current study are similar to results from the European Conditional Mouse Mutagenesis Program (EUCOMM) and the Knockout Mouse Project (KOMP) reporting 461 mouse gene mutations where homozygous mutant mouse lines produced from constructs employing promoter-driven selection (~72% viable following birth including postnatal lethal cases, ~28% embryonic lethal, and ~13% sub-viable postnatally)⁸².

Fig. 2. Gene Mutations that Cause Infertility in Rats

- a) Mean litter size produced by crossing female and male homozygous *Sleeping Beauty* mutant rats (*gt:gt*) with wildtype breeders (WT) (n=18 distinct mutant strains; See details on breeding homozygous mutant rat strains in Supplementary Table 2).
- b) Developmental steps during sperm maturation or fertilization disrupted by respective homozygous genetraps (*tg:tg*) in rats. *Note: *Btrc*^{gt/gt} rats displayed pre-meiotic (~85% tubules) and post-meiotic (~15% tubules) spermatogenic arrest.
- c) Testes from wildtype (Wt) and homozygous genetraps (Mu). Scale bar, 5 mm.

Fig. 3. Pathology Linked to Carboxy Terminal Truncation of Rat ATG13

- a) Diagram of *Sleeping Beauty* β -Geo genetrapp in intron 15 of rat *Atg13*. The genetrapp splices to exon 15 of *Atg13* and is out of frame with the β -Geo reporter. This is predicted to replace the C-terminal 25aa of wildtype ATG13 encoded by exon 16 (ATG13 Δ e16) with a 24aa epitope (blue font) derived from the genetrapp construct, thereby, generating a mutant protein of the same molecular size. *Inset*: (top panel) western blot probing ATG13 in tissues from wildtype (WT) and homozygous mutant *Atg13*^{gt:gt} (Mu) rat littermates; (bottom panel) same blot probed for GAPDH. Arrowheads point to WT and Mu rat proteins with molecular size of ATG13 (~65 kDa) and GAPDH (~37 kDa). Br, brain; SkM, skeletal muscle; Te, testis; Ht, heart; Ki, kidney; Lu, lung; Sp, spleen
- b) Kaplan-Meier estimator of postnatal survival for *Atg13*^{wt:wt} (wildtype), *Atg13*^{wt:gt} (heterozygous) and *Atg13*^{gt:gt} (homozygous) mutant rats.
- c) Liver (top) and Kidney (bottom) from wildtype and homozygous mutant (*Atg13*^{gt:gt}) littermates. Liver scale bar, 2 cm; Kidney scale bar, 5 mm.
- d) Trichrome stained sections illustrating dramatic sclerosis of the glomerular tuft and fibrosis in Bowman's capsule of an *Atg13*^{gt:gt} rat. Note proliferating epithelial cells lining Bowman's capsule (arrows). An adjacent tubule is dilated and filled with protein rich filtrate (asterisks). Kidney sections from wildtype and *Atg13*^{gt:gt} littermates, postnatal D110. Scale bar, 100 μ m.
- e) Forearms of *Atg13*^{gt:gt} phenotype in one strain. Note swelling of left arm and digits. Scale bar, 5 mm.
- f) Relative expression of the autophagy marker proteins LC3a I and LC3a II, and TUBA1a in embryonic fibroblasts derived from wildtype and mutant rats following treatment

with or without combinations of rapamycin, ammonium chloride (NH₄CL₂) and bafilomycin-A1 (BAF-A).

Fig. 4. RNA profiling in mutant *Piccolo* rats

a) Diagram of *Sleeping Beauty* β -*Geo* genetrap in intron 3 of rat *Pclo*. The genetrap splices to exon 3 of *Pclo* and is out of frame with the β -*Geo* reporter. This is predicted to replace the C-terminal 3805aa or 4010aa encoded by exons 4-25 of wildtype PCLO variants (PCLO Δ e4-25) with a 24aa construct-derived epitope (blue font).

b) *Pclo*^{wt:wt}, *Pclo*^{wt:gt} and *Pclo*^{gt:gt} rat mating after pairing with wildtype breeders based on identification of spermatozoa in vaginal swabs. (n) = 8 to 12 total breeder pairs/genotype, or 4 to 6 breeder pairs/sex/genotype for *Pclo*^{wt:gt} and *Pclo*^{gt:gt} mutant strains.

c) Relative abundance (FPKM values) of *Pclo* transcript variants in *Pclo*^{wt:wt}, *Pclo*^{wt:gt} and *Pclo*^{gt:gt} rat brains. †NM_020098, encodes a 4880-amino acid full length isoform; ‡NM_001110797, encodes a 5041-amino acid full length isoform

d) Western blot of Piccolo and TUBA1a in total brain lysates prepared from *Pclo*^{wt:wt}, *Pclo*^{wt:gt} and *Pclo*^{gt:gt} rats.

e) Venn diagram shows the number of differentially expressed genes in the brain, testis or common in both tissues of *Pclo*^{gt/gt} rats when compared to *Pclo*^{wt/wt} rats.

f) Scatter plots of Log₂-fold change for differentially expressed genes (DEGs) in *Pclo*^{wt/gt} (Het) and *Pclo*^{gt/gt} (KO) rat brain (top panel) and testis (bottom panel) compared to wildtype (Wt). Genes that were changed comparably in both heterozygous and homozygous rats, but were differentially expressed (log₂-fold change >1 or <-1; FDR < 0.05), are shown in dark blue. DEGS that changed more in heterozygous or more in homozygous vs wild type are shown in red and blue, respectively (log₂-fold change >1 or <-1; FDR < 0.05). Note that the

Pclo mutation affected more changes in the brain vs testis transcriptome. *Gabra6* and *Gabrg3*, the most significantly affected genes in brain and testis, respectively, have similar expression pattern in the homozygous and heterozygous mutant rats.

Fig. 5. Piccolo deficiency disrupts synaptic transmission and reproduction genes

- a) Ontology of the differentially expressed genes in *Pclo*^{gt/gt} brain vs wildtype. Relative expression of 80 genes, involved in synaptic transmission in *Pclo*^{gt/gt} brain vs wildtype (log₂-fold change >1 or <-1; FDR < 0.05). See *Supplemental Table 6* for lists of most significantly affected Ontology Terms in brain and testes.
- b) Gene Ontology gene enrichment pathway analysis in *Pclo*^{wt/wt} vs *Pclo*^{gt/gt} rat brain clusters downregulated Hormonal Secretion (blue circle & box) and Synaptic Transmission (Red Circle & box) GO: gene sets.
- c) Quantification of the average number of GnRH positive neurons per section within the POA, revealing that the loss of Piccolo does not affect the number of GnRH neurons within the POA.
- d) High magnification images of GnRH positive neurons (Scale bars = 100µm).
- e) Overlap between differentially expressed genes in *Pclo*^{gt/gt} rat testes and genes regulated by gonadotropins in rat testes. FSH, Follicle Stimulating Hormone; LH, Luteinizing Hormone, T, Testosterone. log₂-fold change >1 or <-1; FDR < 0.05
- f) Scatter plots of differentially expressed genes in *Pclo*^{gt/gt} rat testes and genes regulated by gonadotropins in rat testes.

Fig. 6. *Piccolo* deficiency RNA endophenotypes link to depression gene profiles

- a) GWAS on human samples showing that *Pclo* and genes regulated by *Pclo* are among the major loci that are risk factors for MDD.
- b) Dysregulated genes in *Pclo*-KO versus depressed rats. Note the significance level of corelated genes.
- c) Scatter plot DEGs comparison between depression and *Pclo*-KO rat neurons. Red dots are showing reverse pattern of expression.
- d) *Gabra6* as prominent gene dysregulated in *Pclo*-KO rat brains is not detected in Pituitary and Hypothalamus of depressed rat. Depression-related marker *Tph2* shown in comparison.

Fig. 7. Dominant and recessive rat *Piccolo* traits unveiled

- a) Top: Seizure rate/hr recorded in *Pclo*^{wt:wt}, *Pclo*^{wt:gt} and *Pclo*^{gt:gt} rats (n=4 rats/genotype). p<0.001 for *Pclo*^{wt:wt} vs. *Pclo*^{wt:gt} or *Pclo*^{gt:gt} rats; p=0.1 for *Pclo*^{wt:gt} vs. *Pclo*^{gt:gt} rats. Bottom: Representative EEG tracings recorded in *Pclo*^{wt:wt}, *Pclo*^{wt:gt} and *Pclo*^{gt:gt} rats.
- b) Abnormal social behavior in mutant *Pclo* rats. Two examples of time lapse frames showing an agitated *Pclo*^{gt/gt} male lunging defensively at a *Pclo*^{wt/wt} female rat. Abnormal lunging behavior was not observed in *Pclo*^{wt/gt} or *Pclo*^{wt/wt} males.
- c) Diagram of prominent neural connections between the rat olfactory and limbic nervous systems disrupted in *Pclo*^{gt/gt} rats. In rodents, sensory input to the limbic system is mediated predominantly *via* the olfactory system [olfactory epithelia > olfactory nuclei > main and/or accessory olfactory bulb > medial amygdala > bed nucleus of stria terminalis > medial pre-optic hypothalamic nucleus]^{3,4}. Mating pheromones bind olfactory receptors in the olfactory epithelium to elicit pre-copulatory social behaviors including partner investigation,

grooming and courtship as essential responses that signal progression to copulatory and post-copulatory behaviors^{3,4}. Notably, hypothalamic regions innervated by the amygdala and BNST are essential for more downstream pre-copulatory (lordosis), copulatory (mounting, intromission, ejaculation) and post-copulatory (parental care) reproductive behaviors, and are also effectively modulated by sex hormones (estrogen, testosterone)^{3,4}

REFERENCES

1. Yang, L., Comminos, A.N. & Dhillon, W.S. Intrinsic links among sex, emotion, and reproduction. *Cell Mol Life Sci* **75**, 2197-2210 (2018).
2. Chen, P. & Hong, W. Neural Circuit Mechanisms of Social Behavior. *Neuron* **98**, 16-30 (2018).
3. Sokolowski, K. & Corbin, J.G. Wired for behaviors: from development to function of innate limbic system circuitry. *Front Mol Neurosci* **5**, 55 (2012).
4. Petrulis, A. Chemosignals and hormones in the neural control of mammalian sexual behavior. *Front Neuroendocrinol* **34**, 255-267 (2013).
5. Matzuk, M.M. & Lamb, D.J. Genetic dissection of mammalian fertility pathways. *Nat Cell Biol* **4 Suppl**, s41-49 (2002).
6. Matzuk, M.M. & Lamb, D.J. The biology of infertility: research advances and clinical challenges. *Nat Med* **14**, 1197-1213 (2008).
7. Berridge, K.C. & Kringelbach, M.L. Pleasure systems in the brain. *Neuron* **86**, 646-664 (2015).
8. Lebow, M.A. & Chen, A. Overshadowed by the amygdala: the bed nucleus of the stria terminalis emerges as key to psychiatric disorders. *Mol Psychiatry* **21**, 450-463 (2016).
9. Gibbs, R.A., *et al.* Genome sequence of the Brown Norway rat yields insights into mammalian evolution. *Nature* **428**, 493-521 (2004).
10. Vigdal, T.J., Kaufman, C.D., Izsvak, Z., Voytas, D.F. & Ivics, Z. Common physical properties of DNA affecting target site selection of sleeping beauty and other Tc1/mariner transposable elements. *J Mol Biol* **323**, 441-452 (2002).
11. Ivics, Z., Izsvak, Z., Medrano, G., Chapman, K.M. & Hamra, F.K. Sleeping Beauty transposon mutagenesis in rat spermatogonial stem cells. *Nat Protoc* **6**, 1521-1535 (2011).
12. Izsvak, Z., *et al.* Generating knockout rats by transposon mutagenesis in spermatogonial stem cells. *Nat Methods* **7**, 443-445 (2010).
13. Ahmed, M.Y., *et al.* Loss of PCLO function underlies pontocerebellar hypoplasia type III. *Neurology* **84**, 1745-1750 (2015).
14. Choi, K.H., *et al.* Gene expression and genetic variation data implicate PCLO in bipolar disorder. *Biol Psychiatry* **69**, 353-359 (2011).
15. Hek, K., *et al.* The PCLO gene and depressive disorders: replication in a population-based study. *Hum Mol Genet* **19**, 731-734 (2010).
16. Sullivan, P.F., *et al.* Genome-wide association for major depressive disorder: a possible role for the presynaptic protein piccolo. *Mol Psychiatry* **14**, 359-375 (2009).

17. Aragam, N., Wang, K.S. & Pan, Y. Genome-wide association analysis of gender differences in major depressive disorder in the Netherlands NESDA and NTR population-based samples. *J Affect Disord* **133**, 516-521 (2011).
18. Lorenzetti, D., *et al.* A transgenic insertion on mouse chromosome 17 inactivates a novel immunoglobulin superfamily gene potentially involved in sperm-egg fusion. *Mamm Genome* **25**, 141-148 (2014).
19. Alers, S., *et al.* Atg13 and FIP200 act independently of Ulk1 and Ulk2 in autophagy induction. *Autophagy* **7**, 1423-1433 (2011).
20. Alers, S., Wesselborg, S. & Stork, B. ATG13: Just a companion, or an executor of the autophagic program? *Autophagy* **10**, 944-956 (2014).
21. Funakoshi, T., Matsuura, A., Noda, T. & Ohsumi, Y. Analyses of APG13 gene involved in autophagy in yeast, *Saccharomyces cerevisiae*. *Gene* **192**, 207-213 (1997).
22. Suttangkakul, A., Li, F., Chung, T. & Vierstra, R.D. The ATG1/ATG13 protein kinase complex is both a regulator and a target of autophagic recycling in Arabidopsis. *Plant Cell* **23**, 3761-3779 (2011).
23. Waites, C.L., Leal-Ortiz, S.A., Andlauer, T.F., Sigrist, S.J. & Garner, C.C. Piccolo regulates the dynamic assembly of presynaptic F-actin. *J Neurosci* **31**, 14250-14263 (2011).
24. Gundelfinger, E.D., Reissner, C. & Garner, C.C. Role of Bassoon and Piccolo in Assembly and Molecular Organization of the Active Zone. *Front Synaptic Neurosci* **7**, 19 (2015).
25. Cases-Langhoff, C., *et al.* Piccolo, a novel 420 kDa protein associated with the presynaptic cytomatrix. *Eur J Cell Biol* **69**, 214-223 (1996).
26. Fenster, S.D. & Garner, C.C. Gene structure and genetic localization of the PCLO gene encoding the presynaptic active zone protein Piccolo. *Int J Dev Neurosci* **20**, 161-171 (2002).
27. Regus-Leidig, H., *et al.* In vivo knockdown of Piccolino disrupts presynaptic ribbon morphology in mouse photoreceptor synapses. *Front Cell Neurosci* **8**, 259 (2014).
28. Carmel, P.W., Araki, S. & Ferin, M. Pituitary stalk portal blood collection in rhesus monkeys: evidence for pulsatile release of gonadotropin-releasing hormone (GnRH). *Endocrinology* **99**, 243-248 (1976).
29. Watanabe, M., Fukuda, A. & Nabekura, J. The role of GABA in the regulation of GnRH neurons. *Front Neurosci* **8**, 387 (2014).
30. Herbison, A.E. & Moenter, S.M. Depolarising and hyperpolarising actions of GABA(A) receptor activation on gonadotrophin-releasing hormone neurones: towards an emerging consensus. *J Neuroendocrinol* **23**, 557-569 (2011).
31. Ciechanowska, M., Lapot, M., Mateusiak, K. & Przekop, F. Neuroendocrine regulation of GnRH release and expression of GnRH and GnRH receptor genes in the hypothalamus-pituitary unit in different physiological states. *Reprod Biol* **10**, 85-124 (2010).
32. Temple, J.L. & Wray, S. Developmental changes in GABA receptor subunit composition within the gonadotrophin-releasing hormone-1 neuronal system. *J Neuroendocrinol* **17**, 591-599 (2005).
33. Nusser, Z., Sieghart, W. & Somogyi, P. Segregation of different GABAA receptors to synaptic and extrasynaptic membranes of cerebellar granule cells. *J Neurosci* **18**, 1693-1703 (1998).
34. Zhou, W., *et al.* Changes in gene expression in somatic cells of rat testes resulting from hormonal modulation and radiation-induced germ cell depletion. *Biol Reprod* **82**, 54-65 (2010).
35. Rutkoski, N.J., Lerant, A.A., Nolte, C.M., Westberry, J. & Levenson, C.W. Regulation of neuropeptide Y in the rat amygdala following unilateral olfactory bulbectomy. *Brain Res* **951**, 69-76 (2002).

36. Primeaux, S.D. & Holmes, P.V. Olfactory bulbectomy increases met-enkephalin- and neuropeptide-Y-like immunoreactivity in rat limbic structures. *Pharmacol Biochem Behav* **67**, 331-337 (2000).
37. Morales-Medina, J.C., Iannitti, T., Freeman, A. & Caldwell, H.K. The olfactory bulbectomized rat as a model of depression: The hippocampal pathway. *Behav Brain Res* **317**, 562-575 (2017).
38. Wang, D., *et al.* Behavioural and neurochemical features of olfactory bulbectomized rats resembling depression with comorbid anxiety. *Behav Brain Res* **178**, 262-273 (2007).
39. Gereau, R.W.t. & Heinemann, S.F. Role of protein kinase C phosphorylation in rapid desensitization of metabotropic glutamate receptor 5. *Neuron* **20**, 143-151 (1998).
40. Szabo, A. Psychedelics and Immunomodulation: Novel Approaches and Therapeutic Opportunities. *Front Immunol* **6**, 358 (2015).
41. Wray, N.R., *et al.* Genome-wide association analyses identify 44 risk variants and refine the genetic architecture of major depression. *Nat Genet* **50**, 668-681 (2018).
42. Howard, D.M., *et al.* Genome-wide association study of depression phenotypes in UK Biobank identifies variants in excitatory synaptic pathways. *Nat Commun* **9**, 1470 (2018).
43. Wang, Y., *et al.* Genome-wide transcriptome analysis of hippocampus in rats indicated that TLR/NLR signaling pathway was involved in the pathogenesis of depressive disorder induced by chronic restraint stress. *Brain Res Bull* **134**, 195-204 (2017).
44. Mukherjee, K., *et al.* Piccolo and bassoon maintain synaptic vesicle clustering without directly participating in vesicle exocytosis. *Proc Natl Acad Sci U S A* **107**, 6504-6509 (2010).
45. Hieke, N., *et al.* Expression of a ULK1/2 binding-deficient ATG13 variant can partially restore autophagic activity in ATG13-deficient cells. *Autophagy* **11**, 1471-1483 (2015).
46. Takabatake, Y., Kimura, T., Takahashi, A. & Isaka, Y. Autophagy and the kidney: health and disease. *Nephrol Dial Transplant* **29**, 1639-1647 (2014).
47. Zhou, X.J., *et al.* Genetic association of PRDM1-ATG5 intergenic region and autophagy with systemic lupus erythematosus in a Chinese population. *Ann Rheum Dis* **70**, 1330-1337 (2011).
48. Ferreira, R.C., *et al.* Association of IFIH1 and other autoimmunity risk alleles with selective IgA deficiency. *Nat Genet* **42**, 777-780 (2010).
49. Kaizuka, T. & Mizushima, N. Atg13 is essential for autophagy and cardiac development in mice. *Molecular and Cellular Biology* **36**, 585-595 (2016).
50. Henderson, L.P. Steroid modulation of GABAA receptor-mediated transmission in the hypothalamus: effects on reproductive function. *Neuropharmacology* **52**, 1439-1453 (2007).
51. (!!! INVALID CITATION !!! 42-44).
52. Bello, O.D., Zanetti, M.N., Mayorga, L.S. & Michaut, M.A. RIM, Munc13, and Rab3A interplay in acrosomal exocytosis. *Exp Cell Res* **318**, 478-488 (2012).
53. Fenster, S.D., *et al.* Piccolo, a presynaptic zinc finger protein structurally related to bassoon. *Neuron* **25**, 203-214 (2000).
54. Korpi, E.R. & Seeburg, P.H. Natural mutation of GABAA receptor alpha 6 subunit alters benzodiazepine affinity but not allosteric GABA effects. *Eur J Pharmacol* **247**, 23-27 (1993).
55. Kumari, R., *et al.* Potential role of GABAA receptor subunit; GABRA6, GABRB2 and GABRR2 gene polymorphisms in epilepsy susceptibility and pharmacotherapy in North Indian population. *Clin Chim Acta* **412**, 1244-1248 (2011).
56. Hernandez, C.C., Gurba, K.N., Hu, N. & Macdonald, R.L. The GABRA6 mutation, R46W, associated with childhood absence epilepsy, alters β 22 and β 2 GABA(A) receptor channel gating and expression. *J Physiol* **589**, 5857-5878 (2011).

57. Prasad, D.K., *et al.* Association of GABRA6 1519 T>C (rs3219151) and Synapsin II (rs37733634) gene polymorphisms with the development of idiopathic generalized epilepsy. *Epilepsy Res* **108**, 1267-1273 (2014).
58. Yang, L., *et al.* The essential role of hippocampal alpha6 subunit-containing GABAA receptors in maternal separation stress-induced adolescent depressive behaviors. *Behav Brain Res* **313**, 135-143 (2016).
59. Waites, C.L., *et al.* Bassoon and Piccolo maintain synapse integrity by regulating protein ubiquitination and degradation. *EMBO J* **32**, 954-969 (2013).
60. Homanics, G.E., *et al.* Gene knockout of the alpha6 subunit of the gamma-aminobutyric acid type A receptor: lack of effect on responses to ethanol, pentobarbital, and general anesthetics. *Mol Pharmacol* **51**, 588-596 (1997).
61. Jones, A., *et al.* Ligand-gated ion channel subunit partnerships: GABAA receptor alpha6 subunit gene inactivation inhibits delta subunit expression. *J Neurosci* **17**, 1350-1362 (1997).
62. Korpi, E.R., *et al.* Cerebellar granule-cell-specific GABAA receptors attenuate benzodiazepine-induced ataxia: evidence from alpha 6-subunit-deficient mice. *Eur J Neurosci* **11**, 233-240 (1999).
63. Edenberg, H.J. & Foroud, T. The genetics of alcoholism: identifying specific genes through family studies. *Addict Biol* **11**, 386-396 (2006).
64. Dick, D.M., *et al.* Association of GABRG3 with alcohol dependence. *Alcohol Clin Exp Res* **28**, 4-9 (2004).
65. Enoch, M.A., *et al.* GABAergic gene expression in postmortem hippocampus from alcoholics and cocaine addicts; corresponding findings in alcohol-naive P and NP rats. *PLoS One* **7**, e29369 (2012).
66. Robinson, R., *et al.* Linkage analysis between childhood absence epilepsy and genes encoding GABAA and GABAB receptors, voltage-dependent calcium channels, and the ECA1 region on chromosome 8q. *Epilepsy Res* **48**, 169-179 (2002).
67. Hogart, A., Nagarajan, R.P., Patzel, K.A., Yasui, D.H. & Lasalle, J.M. 15q11-13 GABAA receptor genes are normally biallelically expressed in brain yet are subject to epigenetic dysregulation in autism-spectrum disorders. *Hum Mol Genet* **16**, 691-703 (2007).
68. McCauley, J.L., *et al.* A linkage disequilibrium map of the 1-Mb 15q12 GABA(A) receptor subunit cluster and association to autism. *Am J Med Genet B Neuropsychiatr Genet* **131B**, 51-59 (2004).
69. Woudstra, S., *et al.* Piccolo genotype modulates neural correlates of emotion processing but not executive functioning. *Transl Psychiatry* **2**, e99 (2012).
70. Woudstra, S., *et al.* Modulatory effects of the piccolo genotype on emotional memory in health and depression. *PLoS One* **8**, e61494 (2013).
71. Barban, N., *et al.* Genome-wide analysis identifies 12 loci influencing human reproductive behavior. *Nat Genet* (2016).
72. Clark, J.T., Kalra, P.S. & Kalra, S.P. Neuropeptide Y stimulates feeding but inhibits sexual behavior in rats. *Endocrinology* **117**, 2435-2442 (1985).
73. Paredes, R.G., Highland, L. & Karam, P. Socio-sexual behavior in male rats after lesions of the medial preoptic area: evidence for reduced sexual motivation. *Brain Res* **618**, 271-276 (1993).
74. Goyal, S.N., Upadhyay, M.A., Kokare, D.M., Bhisikar, S.M. & Subhedar, N.K. Neuropeptide Y modulates the antidepressant activity of imipramine in olfactory bulbectomized rats: involvement of NPY Y1 receptors. *Brain Res* **1266**, 45-53 (2009).
75. Ishida, H., *et al.* Infusion of neuropeptide Y into CA3 region of hippocampus produces antidepressant-like effect via Y1 receptor. *Hippocampus* **17**, 271-280 (2007).

76. Kennedy, S.H. & Rizvi, S. Sexual dysfunction, depression, and the impact of antidepressants. *J Clin Psychopharmacol* **29**, 157-164 (2009).
77. Giniatullina, A., *et al.* Functional characterization of the PCLO p.Ser4814Ala variant associated with major depressive disorder reveals cellular but not behavioral differences. *Neuroscience* **300**, 518-538 (2015).
78. Ivics, Z., *et al.* Transposon-mediated genome manipulation in vertebrates. *Nat Methods* **6**, 415-422 (2009).
79. Jiang, H. & Wong, W.H. Statistical inferences for isoform expression in RNA-Seq. *Bioinformatics* **25**, 1026-1032 (2009).
80. Mortazavi, A., Williams, B.A., McCue, K., Schaeffer, L. & Wold, B. Mapping and quantifying mammalian transcriptomes by RNA-Seq. *Nat Methods* **5**, 621-628 (2008).
81. Anders, S. & Huber, W. Differential expression analysis for sequence count data. *Genome Biol* **11**, R106 (2010).
82. Ayadi, A., *et al.* Mouse large-scale phenotyping initiatives: overview of the European Mouse Disease Clinic (EUMODIC) and of the Wellcome Trust Sanger Institute Mouse Genetics Project. *Mamm Genome* **23**, 600-610 (2012).

Figure 1

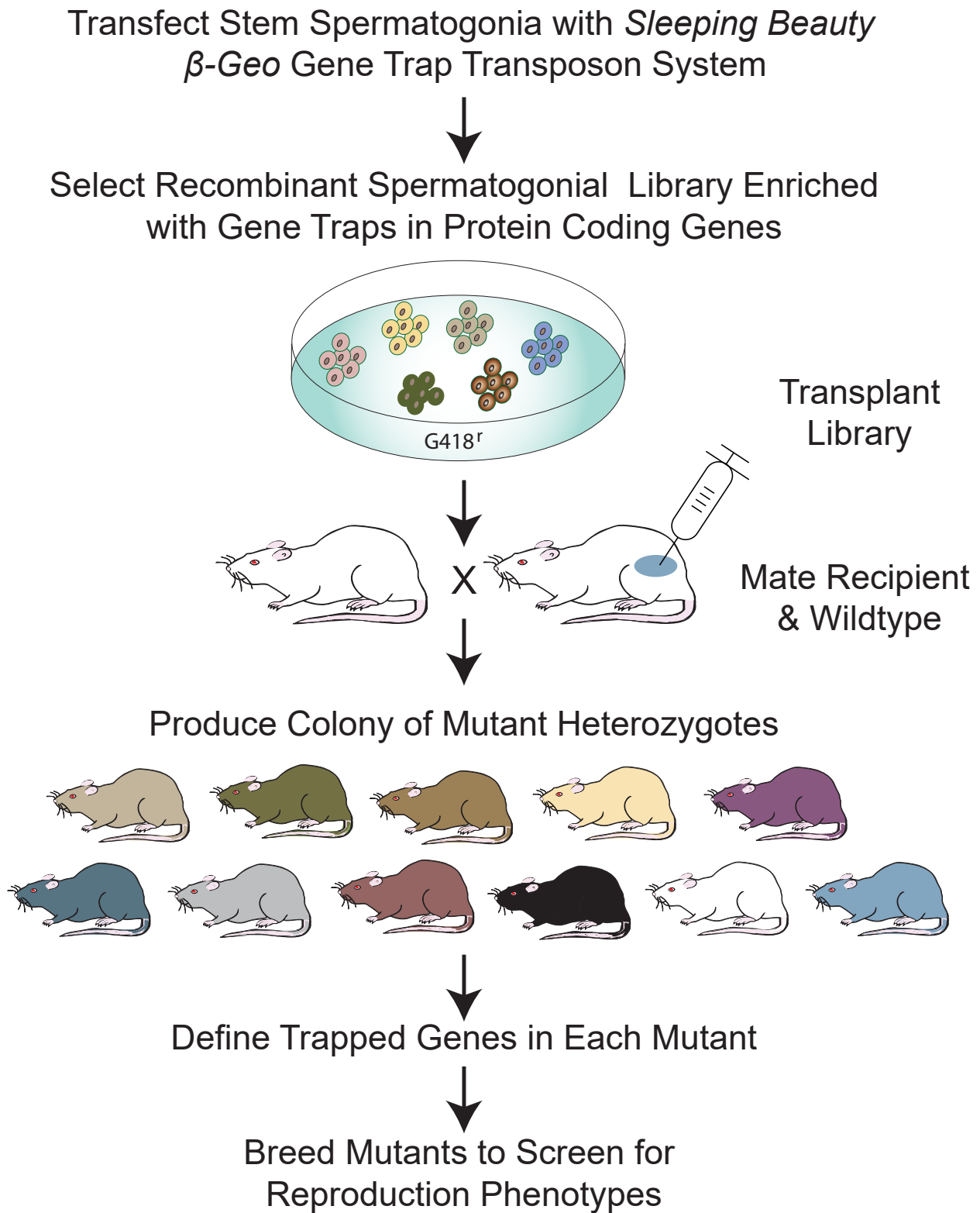


Figure 2

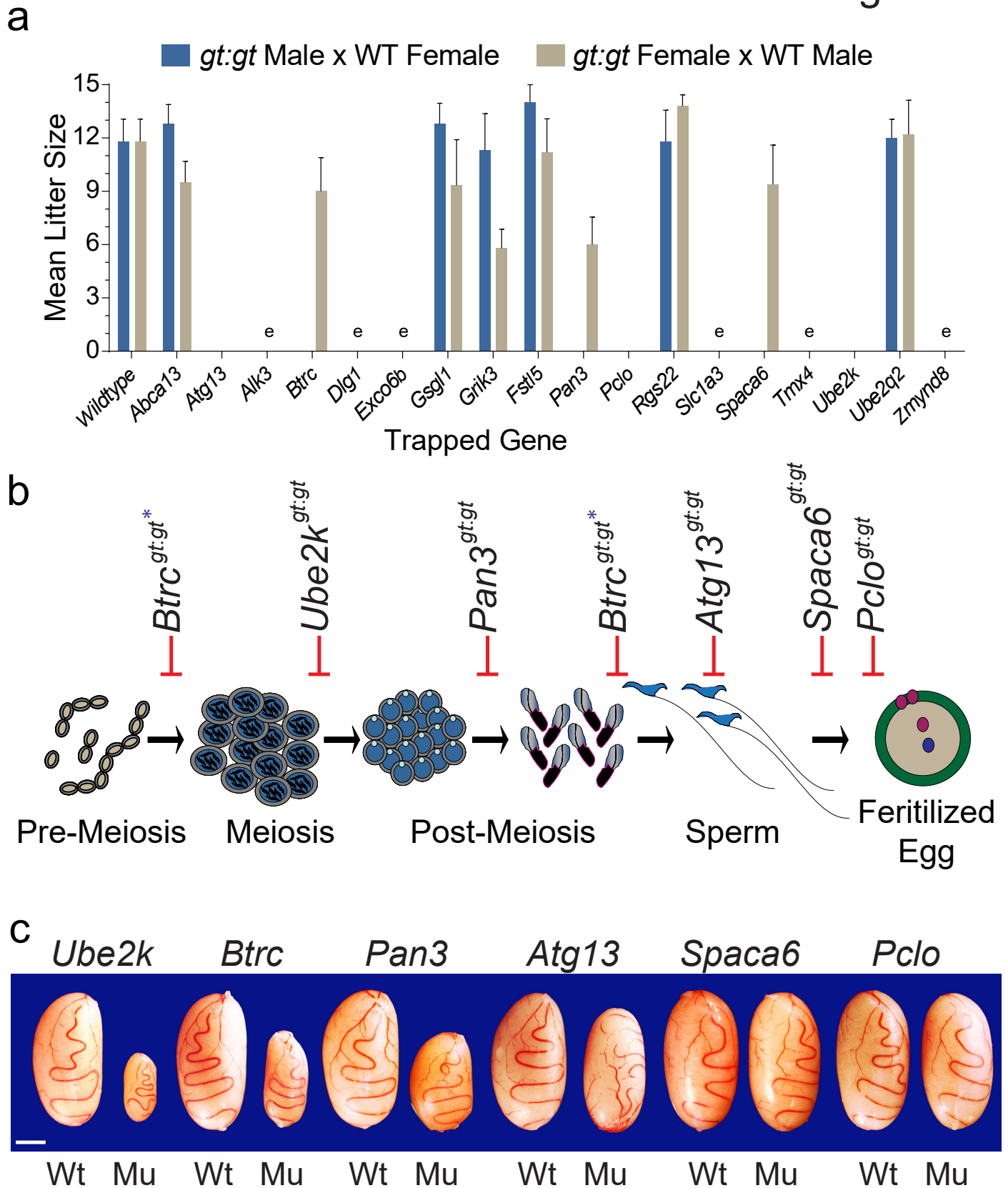


Figure 3

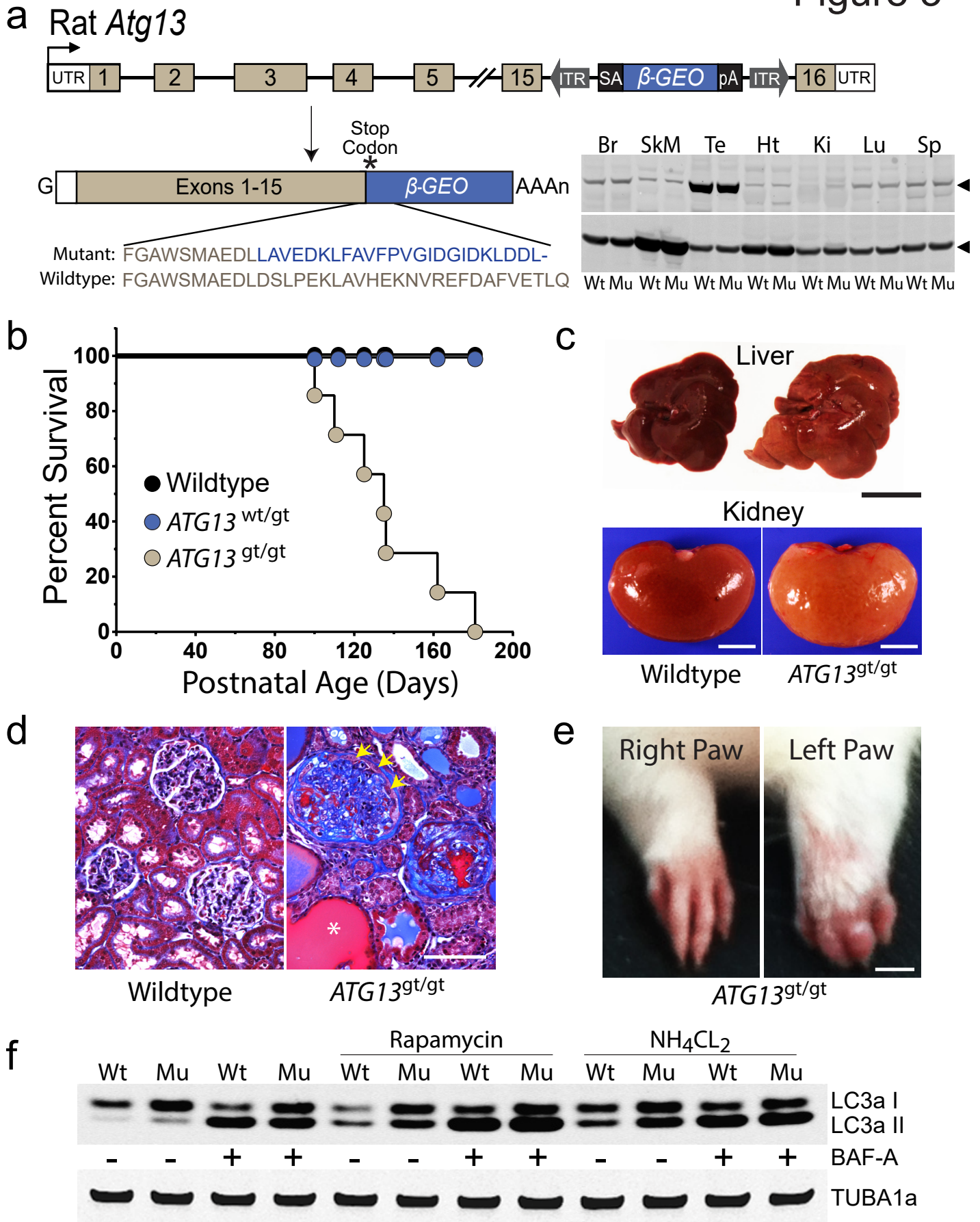


Figure 4

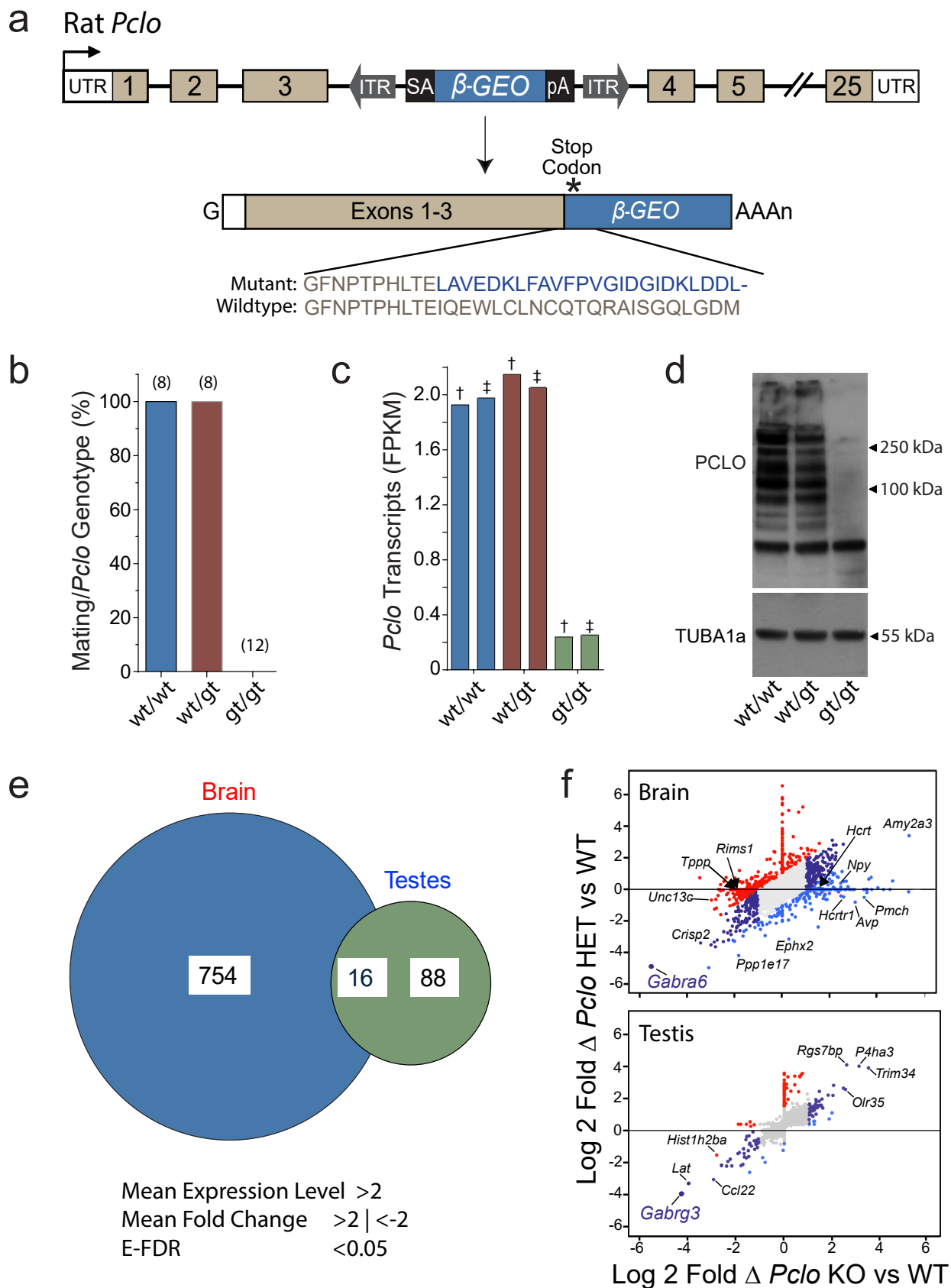


Figure 5

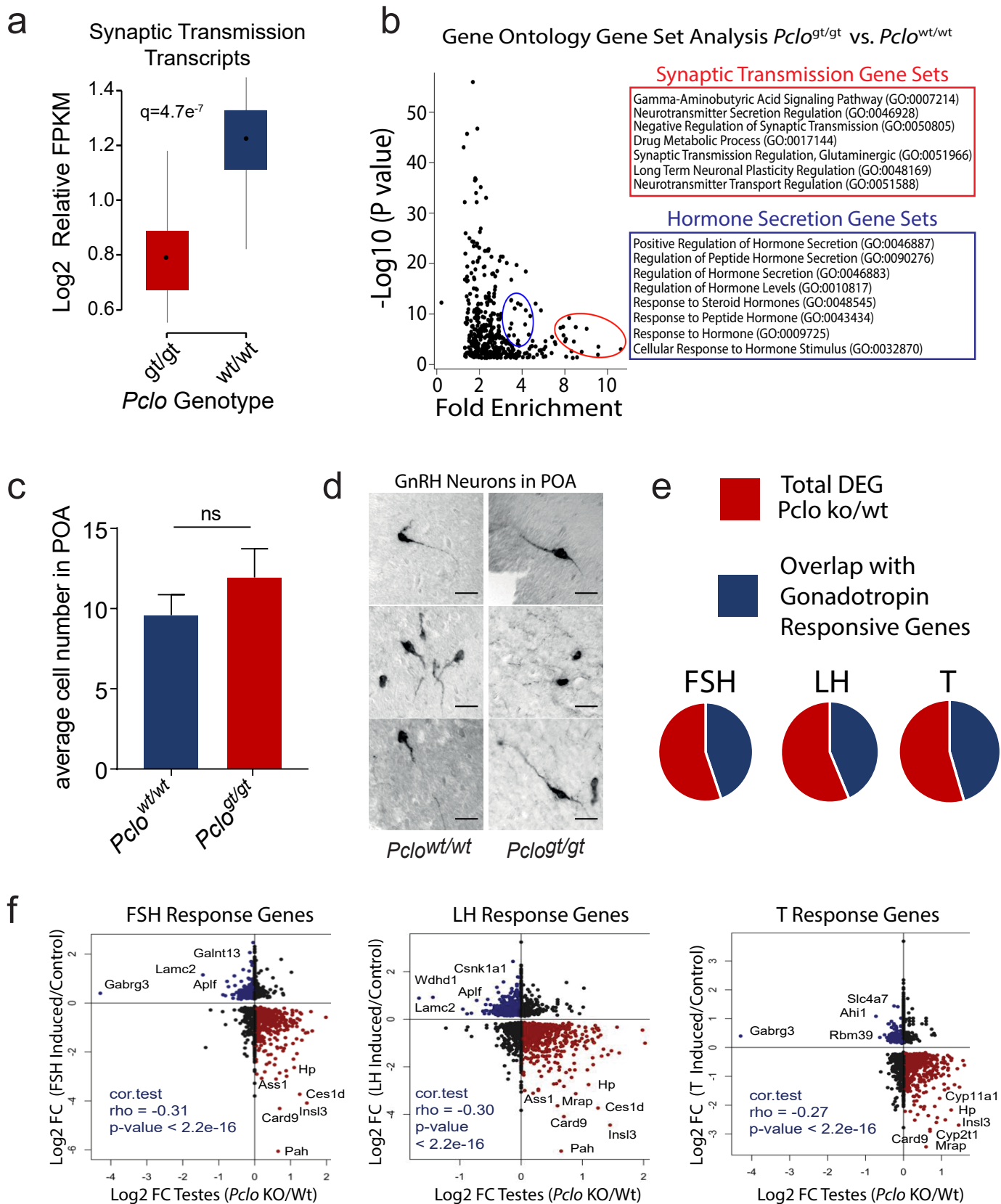


Figure 6

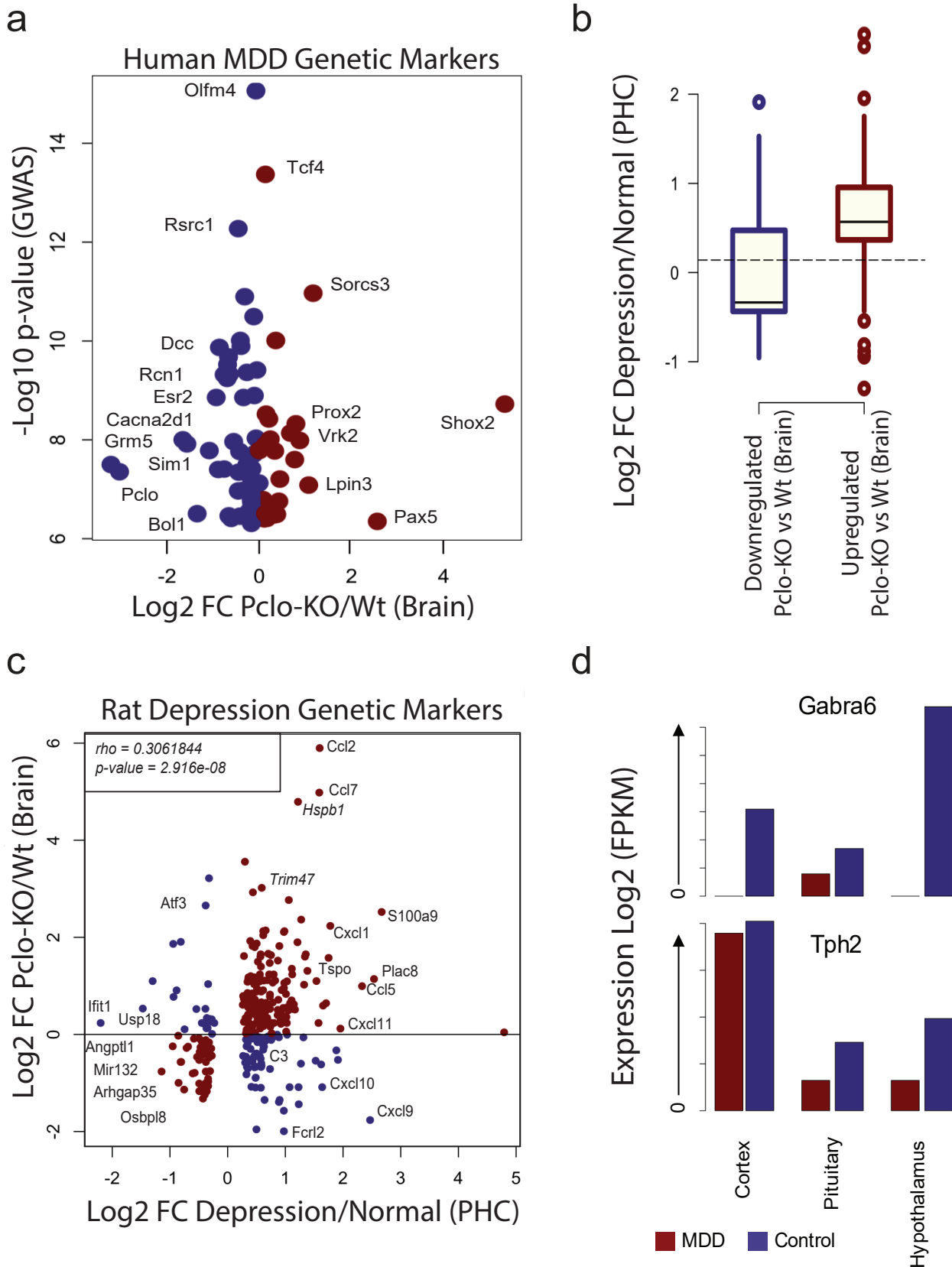
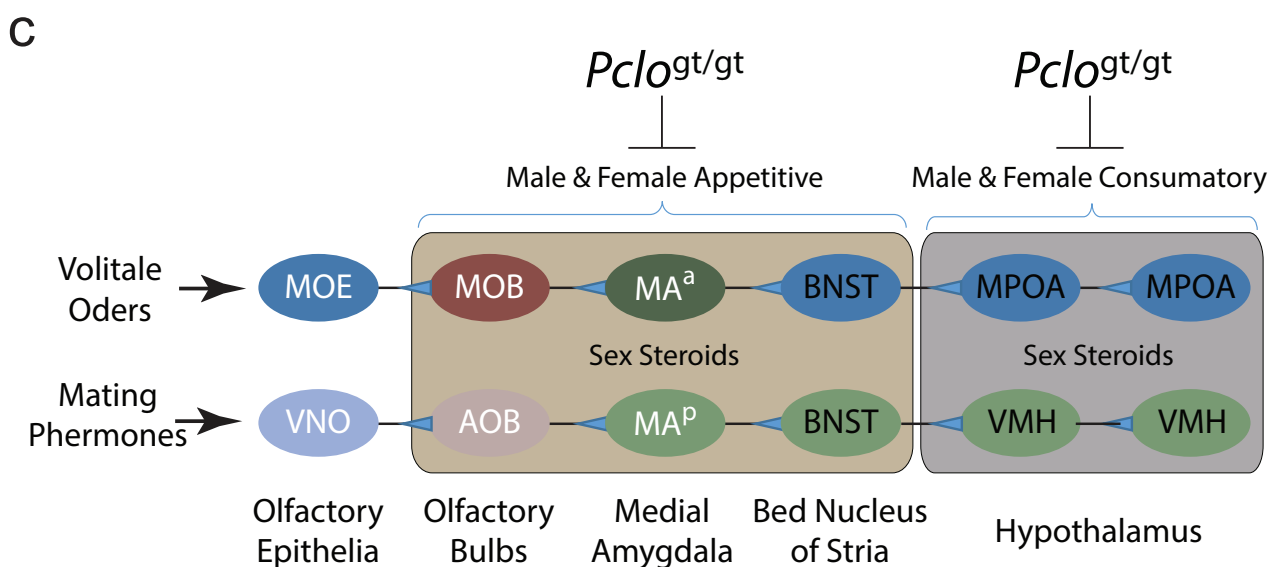
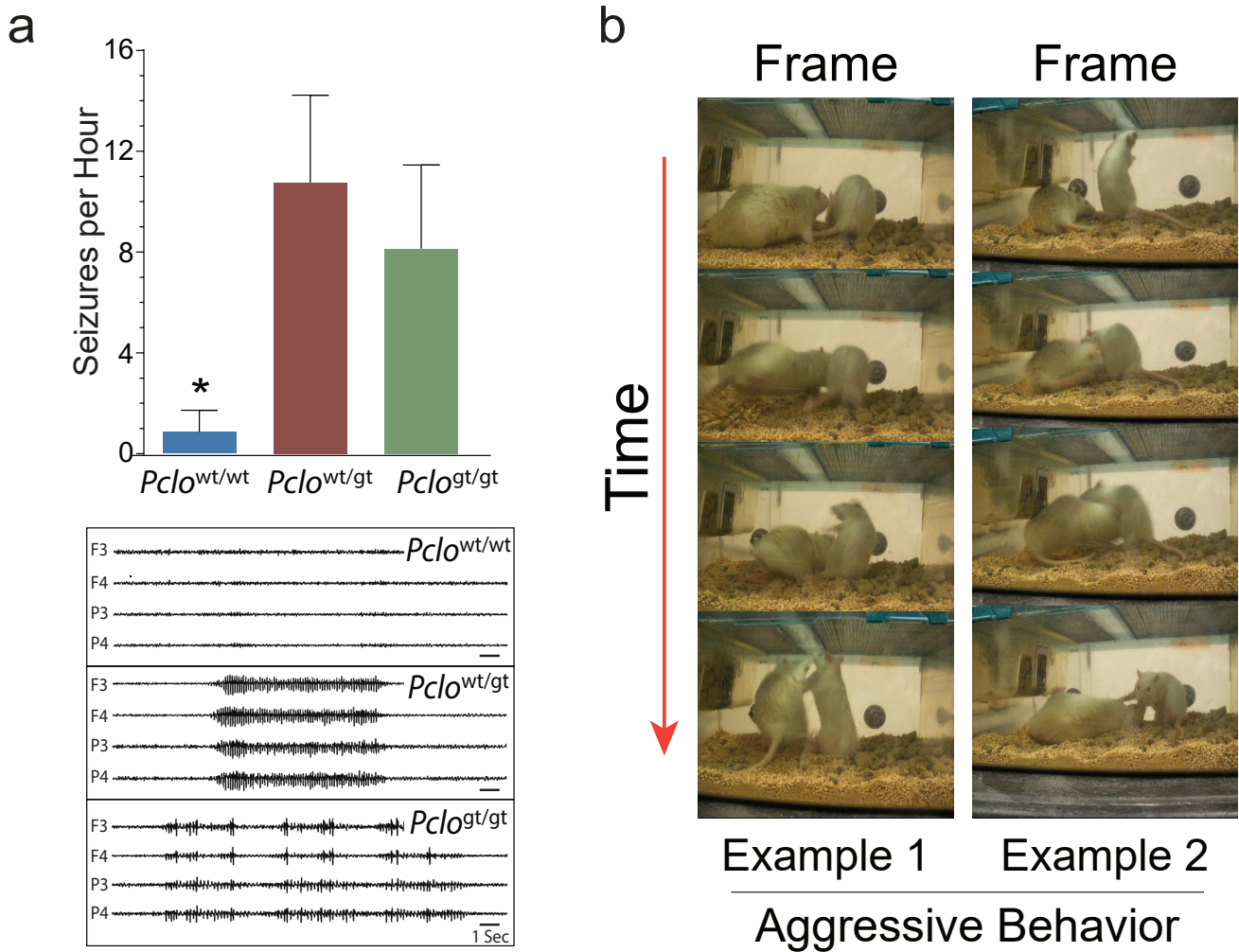
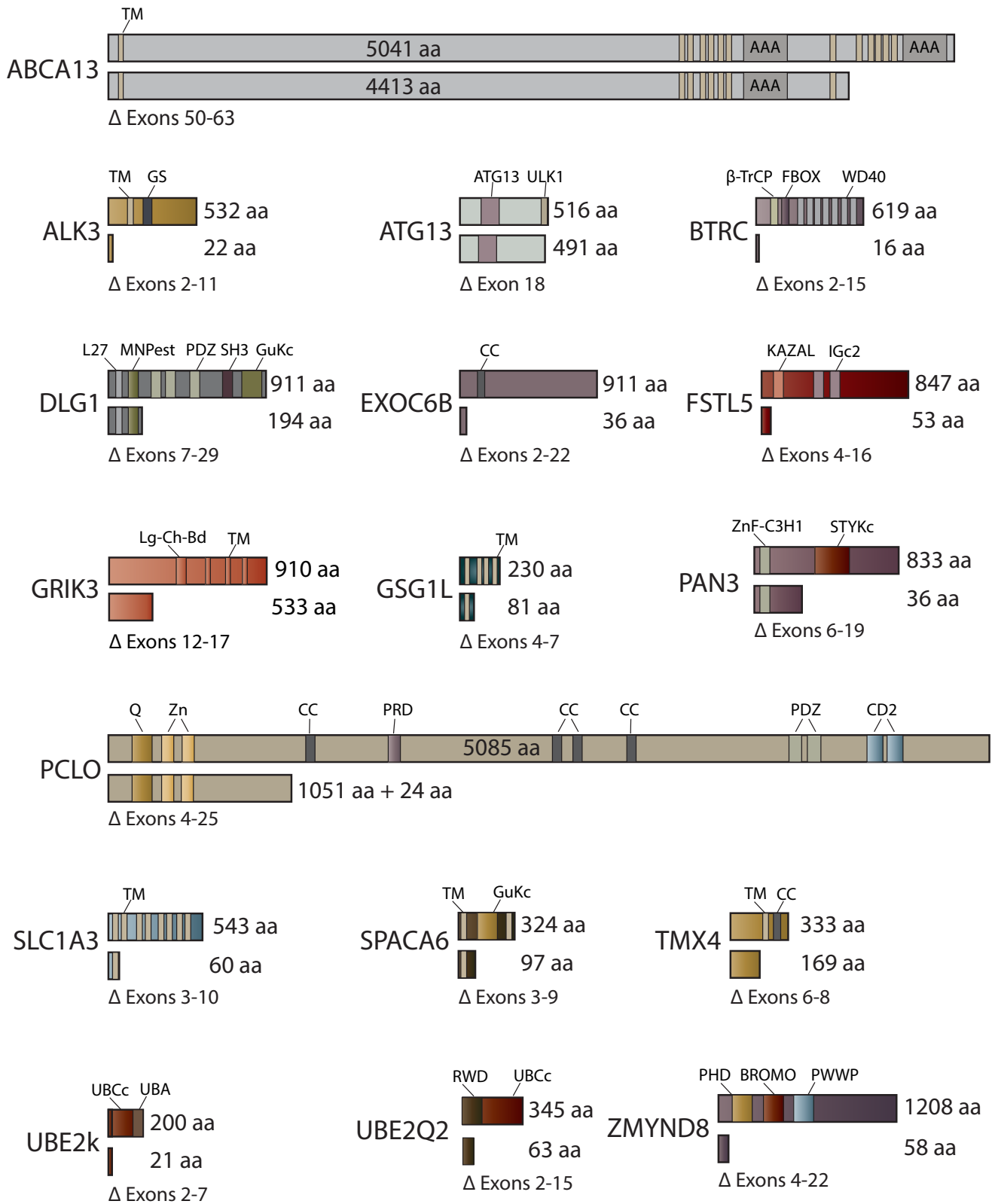


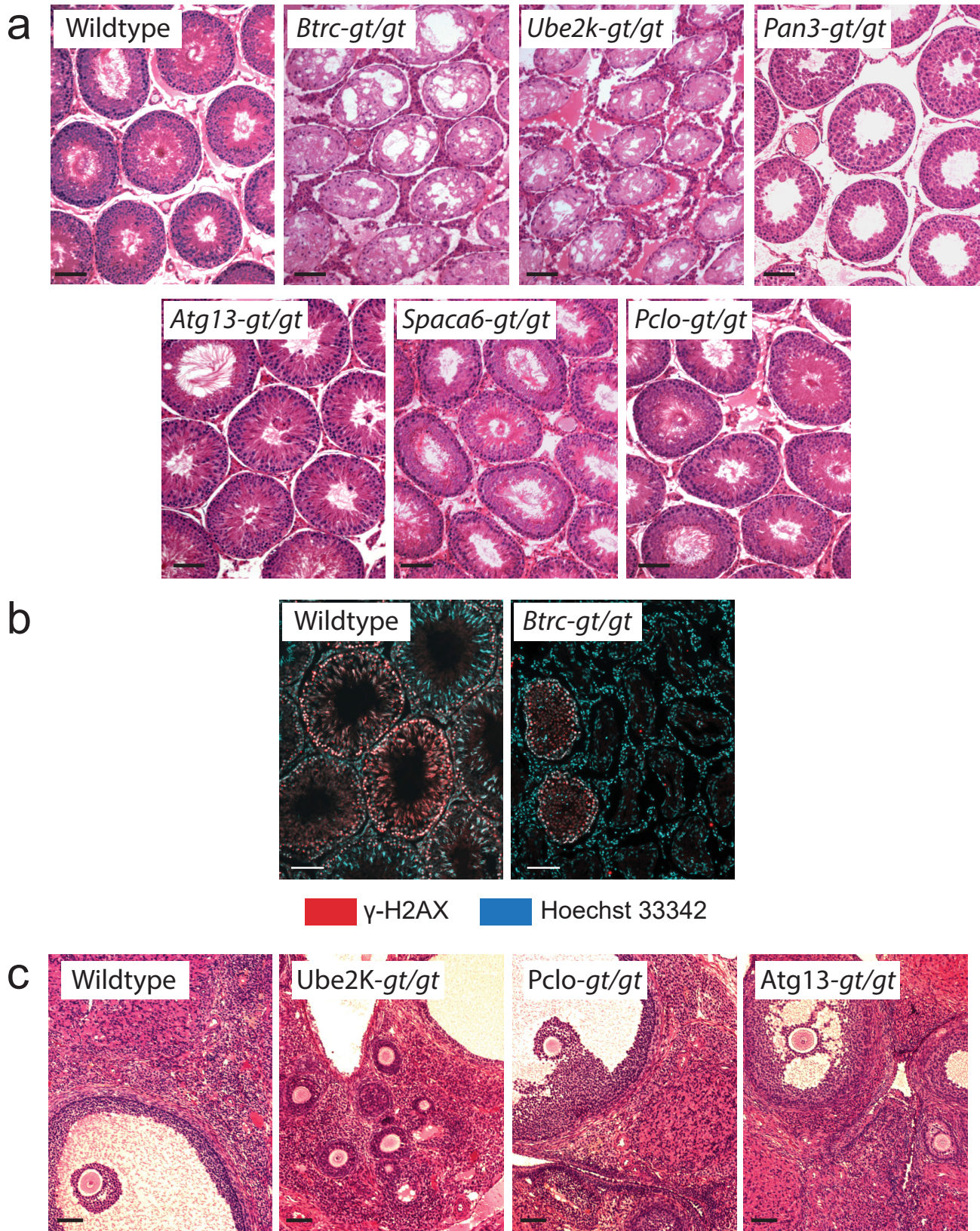
Figure 7



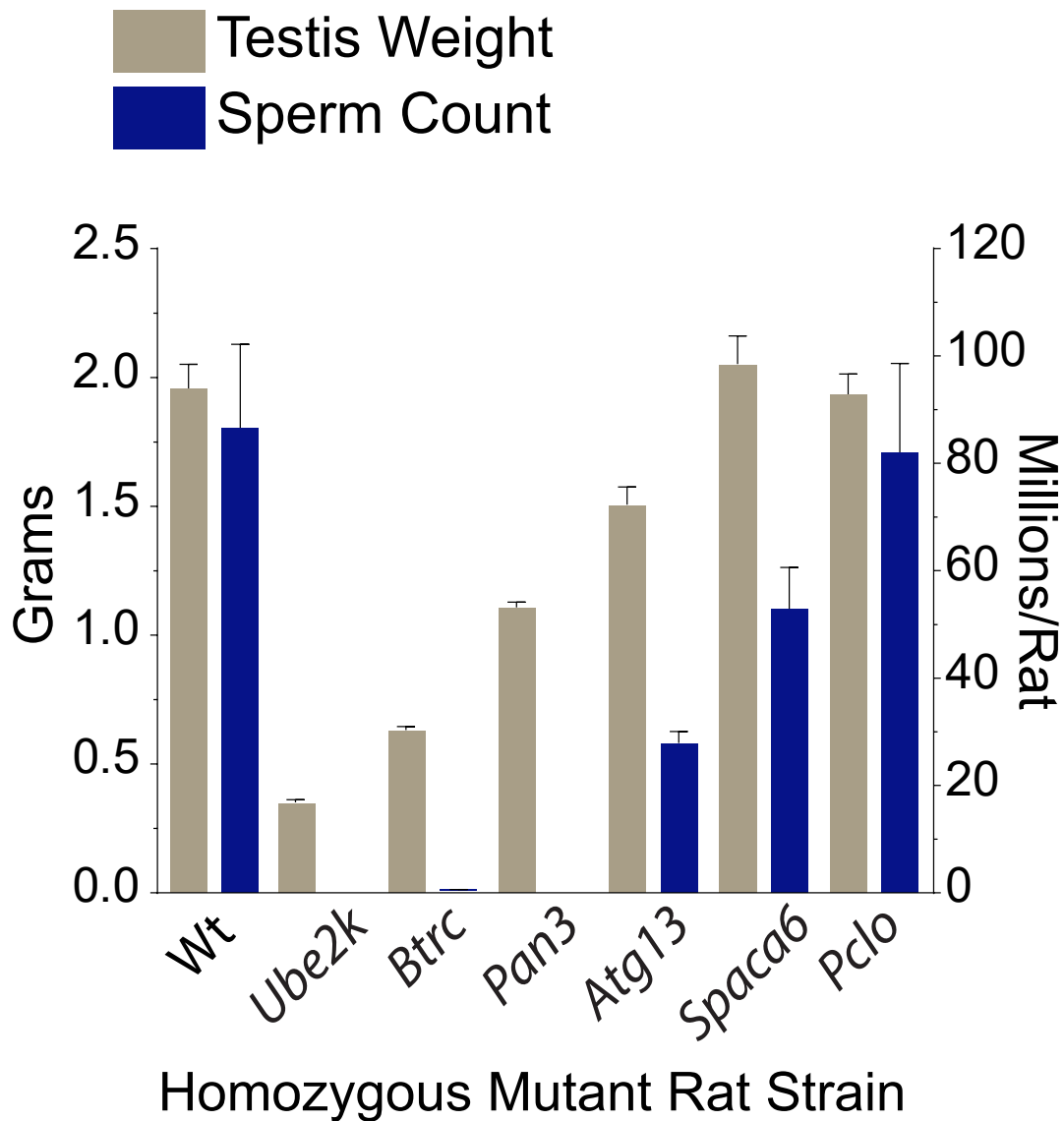
Supplementary Figure 1



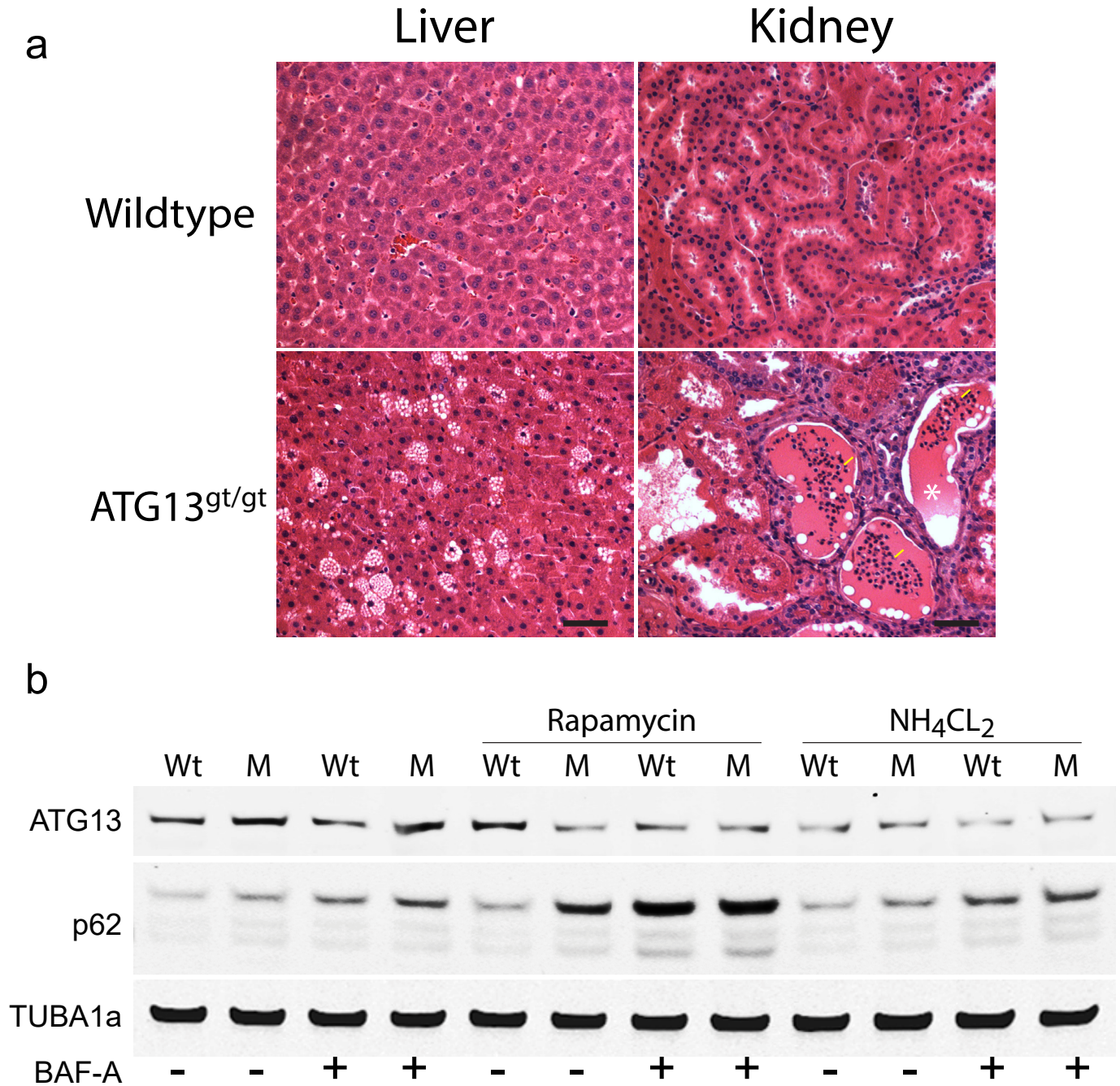
Supplementary Figure 2



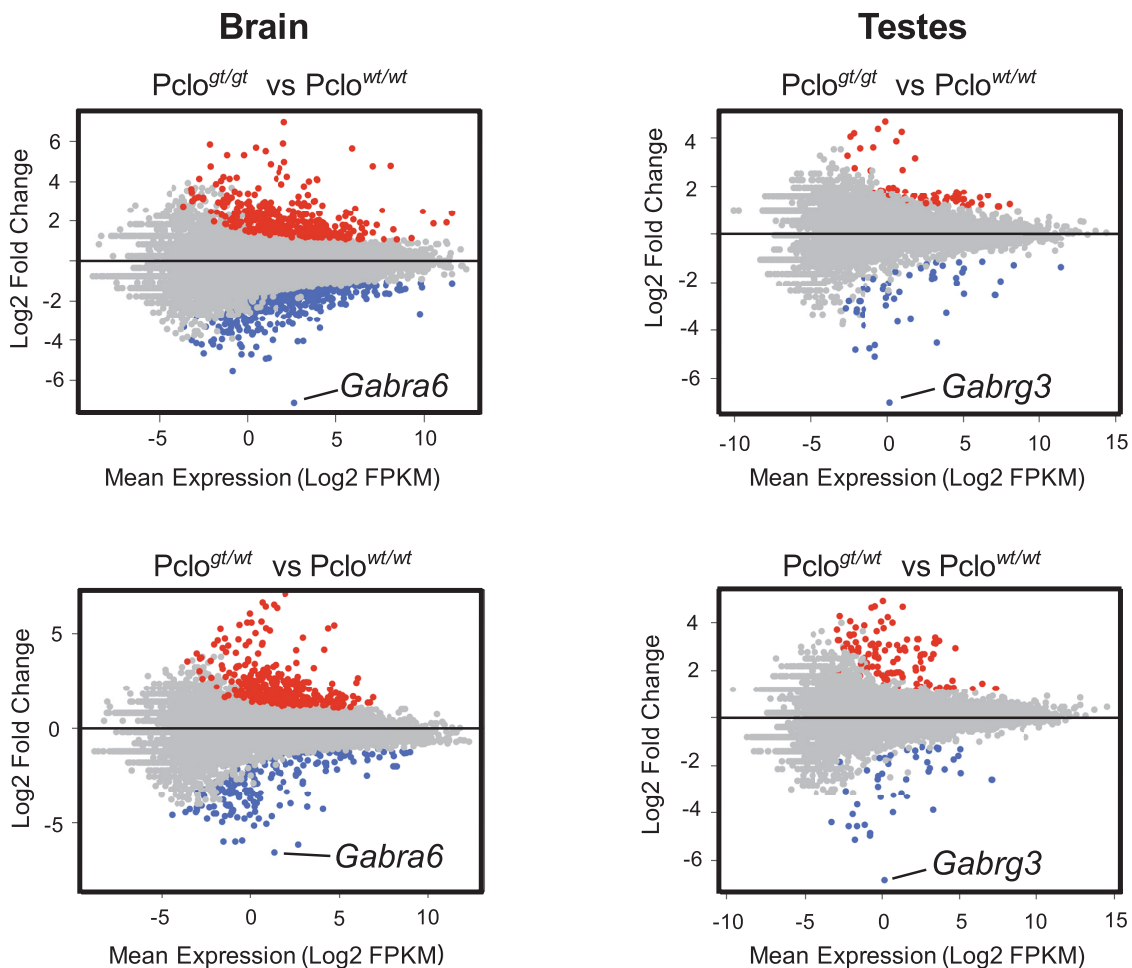
Supplementary Figure 3



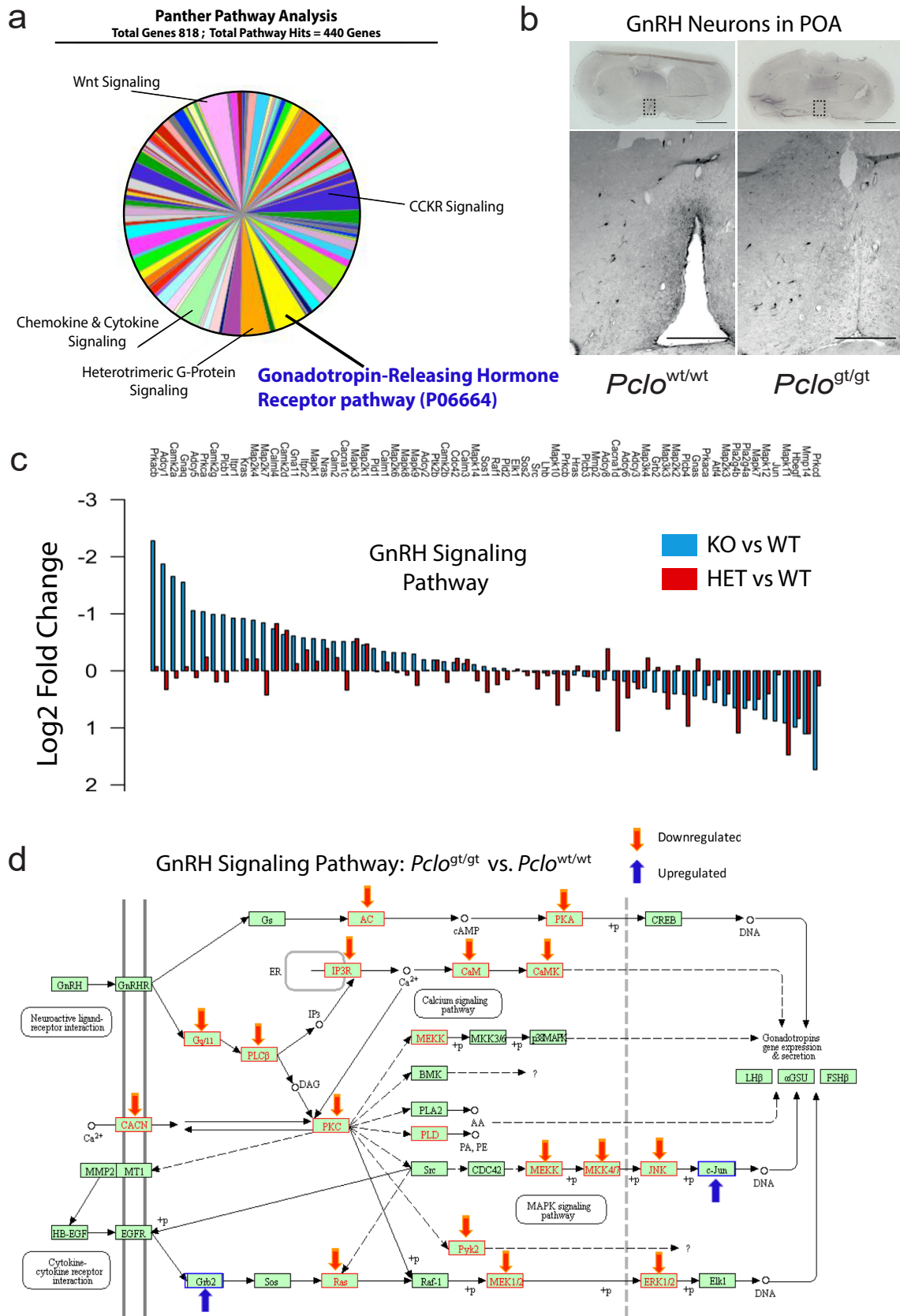
Supplementary Figure 4



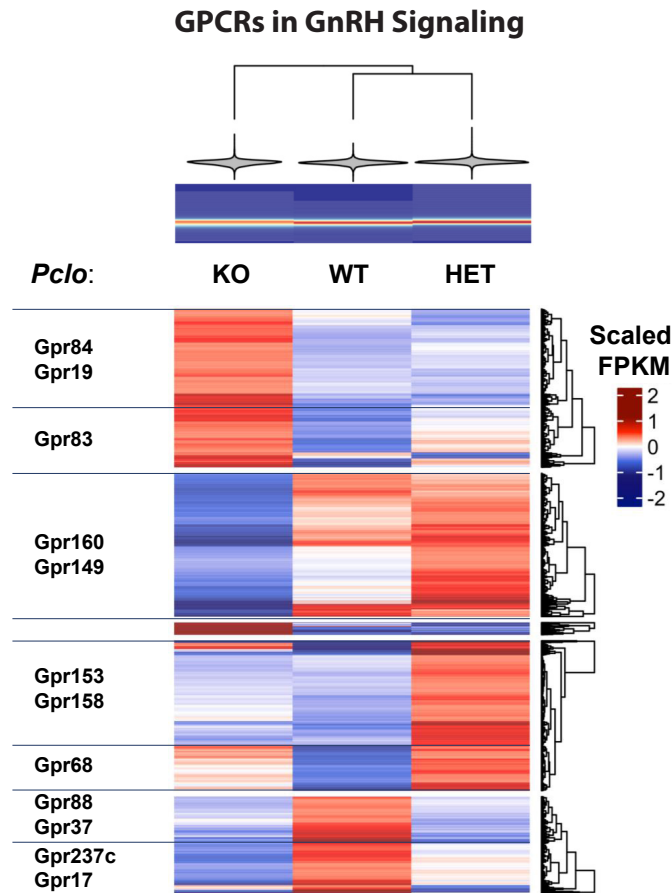
Supplementary Figure 5



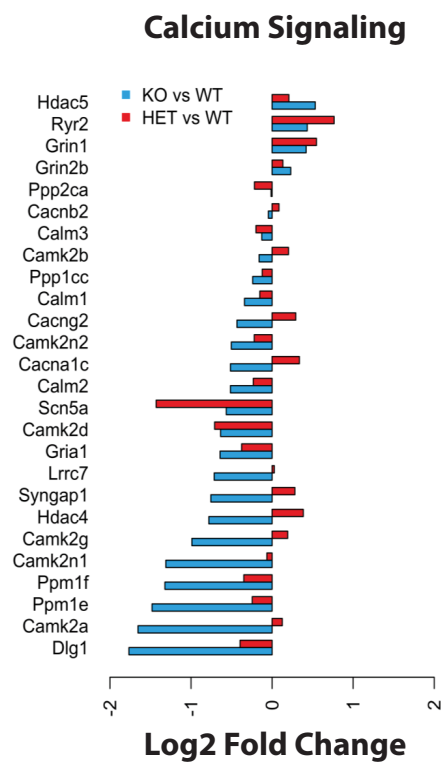
Supplementary Figure 6



a



b



c

